ChemElectroChem

Review
doi.org/10.1002/celc.202400370

Chemistry
Europe
European Chemical
Societies Publishing

www.chemelectrochem.org

Electroanalytical Overview: Screen-Printed Electrochemical Sensing Platforms

Robert D. Crapnell[a] and Craig E. Banks*[a]

Screen-printed electrochemical sensing platforms are ubiquitous within the field of electrochemistry where they provide benefits of being disposable, cost-effective, reproducible, easily customisable, portable and allow one to transfer the laboratory approach into the field. In this review, we introduce the concept of screen-printed electrodes, we summarise positive and negative aspects before moving into the current highlights of using traditional screen-printed carbon electrodes within the field of electroanalysis. We then look to cover metallic and bulk modified varieties, geometric changes (micro, microband and associated arrays), electrode activation and finally the physical length of screen-printed electrodes, providing insights for future research.
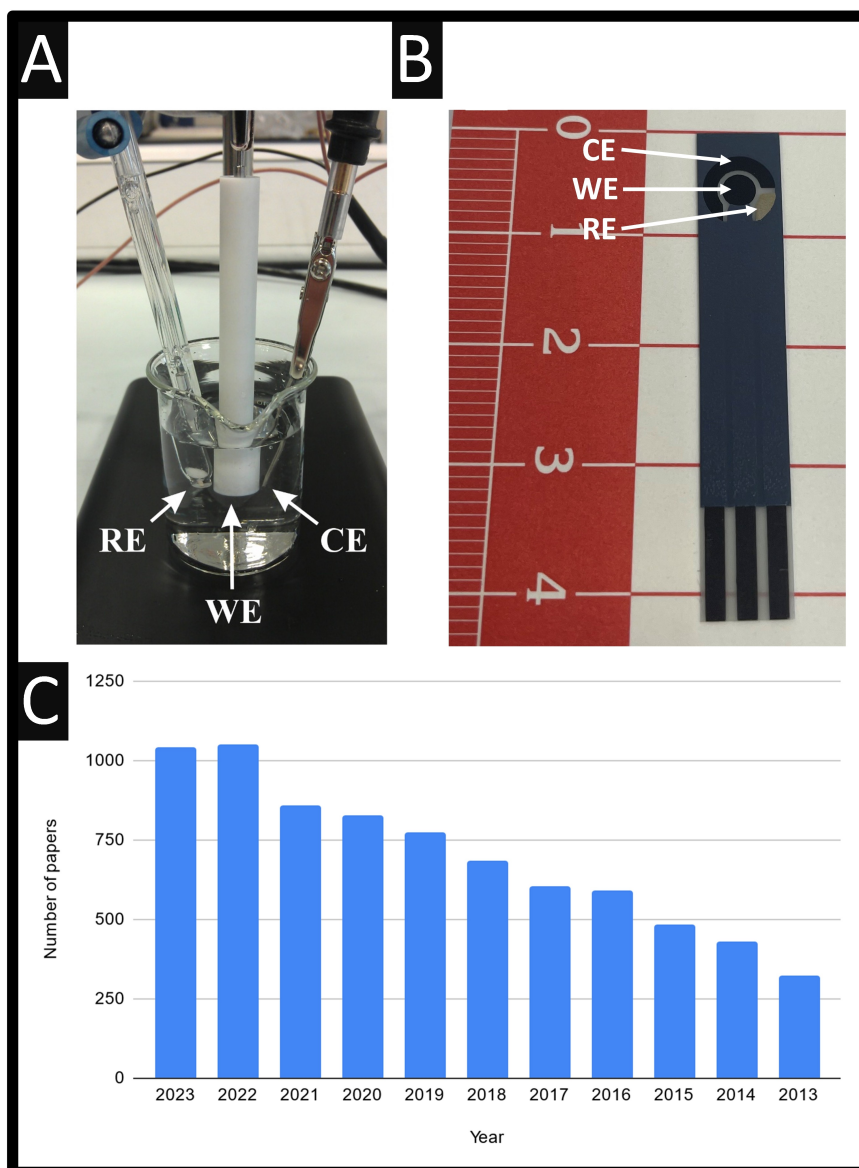
1. Introduction to Screen-Printed Electrochemical Platforms

A classical electrochemical experimental set up is presented in Figure 1A, where we can observe that a commercially available solid glassy carbon working (3 mm diameter, WE), counter (CE) and reference (RE) electrodes are submerged within a solution of interest. This is the backbone of electrochemistry and gives rise to useful electrochemical and electroanalytical results. With these electrodes, one might need to replenish the surface of the working electrode via electrode cleaning (electrochemically) and/or polishing between intra-experimental measurements due to the possible adsorption of species or ions and during inter-experimental measurements to remove memory efforts that can result in cross-contamination. One way around this is the use of screen-printed graphite electrodes, see Figure 1B, which have shown to provide the same electrochemical measurements but has the following benefits:[1–15] 1. *Cost-effectiveness*: screen-printed electrodes are relatively inexpensive to produce compared to traditional solid electrodes, making them accessible for research and industrial applications due to their scale of economy; 2. *Disposable*: since they are inexpensive, screen-printed electrodes are often disposable, eliminating the need for cleaning and reduces the risk of cross-contamination between samples; 3. *Miniaturization and low volumes*: screen-printed electrodes can be made with smaller electrodes working in a small overall area which lends the use of screen-printed electrodes where it is an advantage to have a small sample volume allowing for miniaturization of devices. The classic use combining the synergy of microfluidics and biosensing is the capillary fill screen-printed electrodes where a sample volume of less than 4 microlitres and have the advantage of self-filling which is particularly useful in portable and point-of-care diagnostic tools; 4. *Multiple sensing*: due to the small size of screen-printed electrodes, multiple analytes can be measured within a single sample–for example six or more screen-printed electrodes can be used for the sensing of analytes. 5. *Versatility*: These can be made with a variety of materials, such as carbon, metals, or metal oxides, allowing for customization based on the specific application's needs; 6. *Ease of fabrication*: screen-printed electrodes are fabricated using screen-printing technology, which is a simple and scalable process. This means they can be mass-produced with high reproducibility; 7. *Compatibility*: screen-printed electrodes are compatible with a wide range of analytical techniques, including voltammetry, amperometry, impedance spectroscopy, and much more; 8. *Highly reproducible*, but yet, giving rise to fast electron transfer rates which are comparable to solid carbon electrodes, for example, the using the near-ideal outer sphere redox probe hexaamineruthenium (III) chloride/0.1 M KCl, an order of magnitude is commonly found (10^{-3} cm s^{-1})[16] which is comparable, for example using glassy carbon electrodes (10^{-2} cm s^{-1})[17]–noting that the a glassy carbon is a homogeneous surface is predominantly carbon compared to a screen-printed electrode which is made up of conductive material, solvents and polymeric binders;[10,18] 9. *Portable* and allows one to transfer the laboratory approach (Figure 1A) into the field (Figure 1B). Furthermore, smartphone integration improves the functionality of screen-printed electrochemical sensors for real-world use. 10. *Commercialisation:* the use of screen-printed electrodes in the first instance when developing a sensor, allows researchers to consider commercialisation sooner rather than later, making the sensor work on a carbon solid electrode which will need to be reengineered onto screen-printed electrodes. 11. *Ready to use:* solid electrodes need to be pre-treated by mechanically polishing, for example using alumina slurries. Screen-printed electrodes can be fabricated, which are stored in air-tight bags, which allows researchers to open a fresh, ready to use screen-printed electrode. Another example

[a] R. D. Crapnell, C. E. Banks
Faculty of Science and Engineering, Manchester Metropolitan University, Chester Street, Manchester M1 5GD, Great Britain
+441612471196
E-mail: c.banks@mmu.ac.uk

ChemElectroChem

Review

doi.org/10.1002/celc.202400370

Chemistry Europe
European Chemical
Societies Publishing

Figure 1. A: A typical experimental set-up showing the working electrode (WE, glassy carbon, 3 mm diameter), a counter electrode (CE, a nickel wire) and a reference electrode (RE, saturated calomel electrode); **B**: A screen-printed graphite electrode with a working electrode (3.1 mm diameter), a graphite counter and a Ag/AgCl reference electrodes; **C**: A Scopus search of the words "screen printed", AND "electrodes" showing the number of paper published according to the year.

where screen-printed electrodes are useful is the case of solid electrodes where they need to be pre-treated between *inter*-

measurements removing memory effects; a new screen-printed electrode can be used each time. Last, the use of screen-printed

Robert D. Crapnell achieved both his MChem and PhD from the University of Hull, United Kingdom, respectively, in 2014 and 2018. He is currently Technical Facility Manager for Electrochemistry and Polymer Science at Manchester Metropolitan University, United Kingdom. His research is predominantly focused on fundamental electrochemistry, electroanalysis, additive manufacturing electrochemistry, sustainability, and bespoke filament production.

Craig E. Banks holds a personal chair in chemistry and has published over 600 papers and works on next generation screen-printed and additive manufacturing electrochemical sensing platforms.

ChemElectroChem | Review
doi.org/10.1002/celc.202400370

Chemistry
Europe
European Chemical
Societies Publishing

electrodes also overcome *intra*-measurement where there might be highly absorbing species which decreases the electrochemical signal which can be overcome by using a new screen-printed electrode for each measurement helping to speed up the overall analysis time, which is slower when using solid electrode where between each measurement the electrode needs to be subjected to mechanical polishing. 12: *Different surfaces:* classically, graphitic screen-printed electrodes were the first reported which have been extending to metallic electrode surfaces, but others have been over the years these have been extended, for example multi-walled carbon nanotubes, graphene, MXenes and so-on; 13: *Comparable to gold standard laboratory approaches:* There are many examples of where screen-printed electrodes have been shown to be useful for a target analyte, for example an analyte within a human serum sample, where this has directly correlated with independent gold standard laboratory methodology, *i.e.* LC–MS; Screen-printed electrodes find use within the following fields: biosensing,[19,20] medical diagnostics,[21] environmental monitoring,[22,23] food safety,[24] fuel cells,[25] supercapacitors,[26] trace analysis,[27] forensics,[28] water quality,[14] soil analysis,[29] and microbiology.[30] In summary, due to their advantage (see above) of utilising screen-printed electrodes are a go-to-choice for many researchers and industries involved in electrochemical and sensing applications. As shown within Figure 1C, we can see how many researchers have used screen-printed electrodes where in 2013 there was reported 323 papers but 10 years on, this has increased to 1042 indicating a percentage change of 223%.
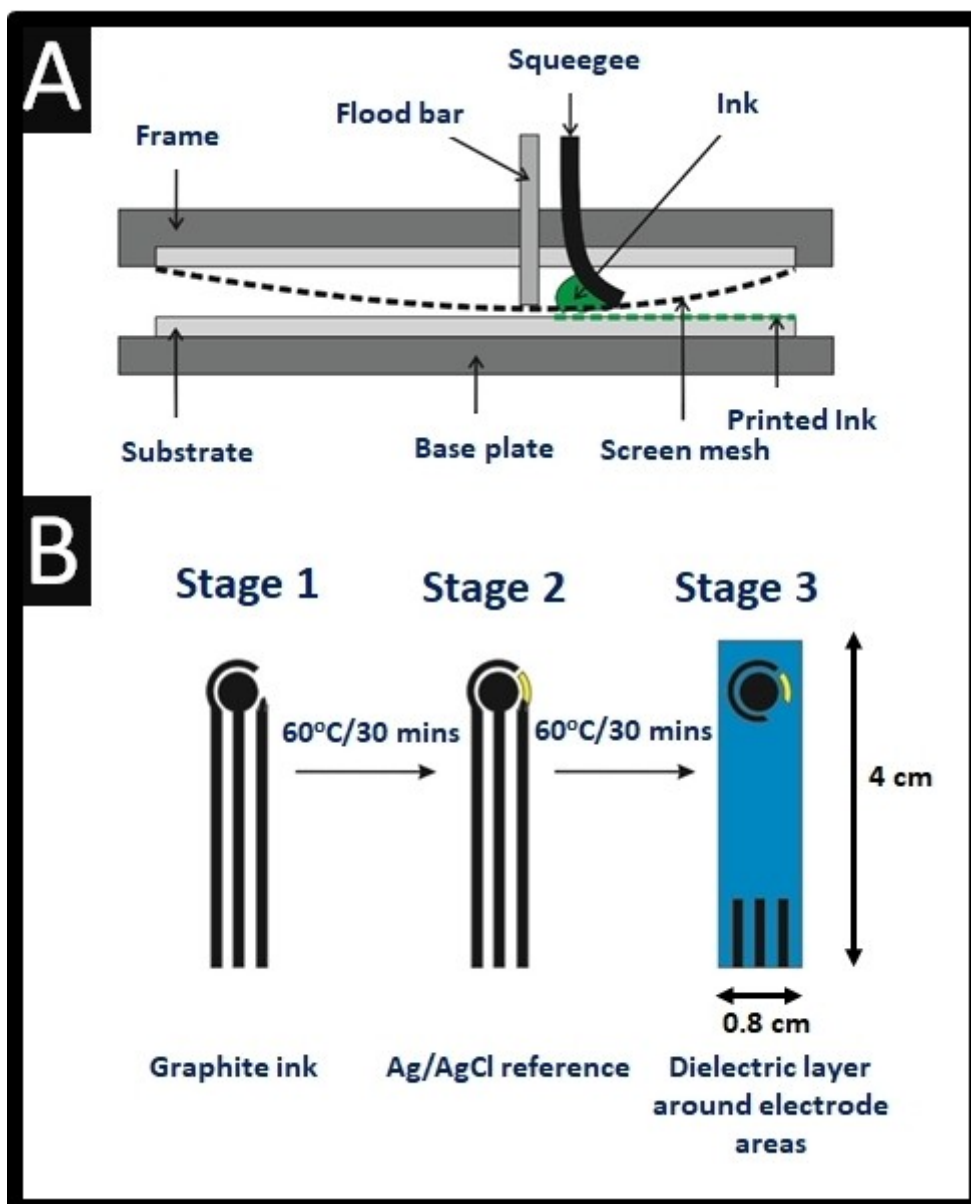
The design and fabrication of screen-printed electrodes comprises the following steps[31]: i) first the design of the geometry and size of the electrode needs to be decided and the corresponding mesh needs to be fabricated. One of the most important parameters of the screen is the mesh counts, or the number of wires per unit length. Another parameter is the size of the opening in the screen which allows (or doesn't) the amount of paste that can be transferred during the printing processes and limits the maximum particle size. In this way the opening, O, is dependent on both the mesh sizes: $O = 1/M–D$, where D is the diameter of the wire and M is the mesh count.[31] The amount of paste that is being screen-printed is dependent on the volume of the opening in the screen assuming that the thickness of the mesh is 2X the wire diameter, the volume, V, is given by: $V = 2D(1/M–D)$.[2,31] ii) Next, the selection and preparation of the conductive and non-conductive inks needs to be completed, along with the selection of the substrate material. Screen printing inks are non-Newtonian fluids with pseudo-plastic (shear thinning) and thixotropic (viscosity decreases over shear time) properties contains a plethora of substances including graphite, carbon black, solvents and polymeric binders.[10,18] The criterial parameters of the inks are the ratio of the solid content, the particle size distribution and the viscosity. These are important when researchers are making their own ink or modifying commercially available ink (see later bulk modified screen-printed electrodes). As shown within Figure 2A, one can observe the screen-printing process where a conductive (graphite) ink is forced through a screen mesh that defines the screen-

printed electrodes via the application of a moving squeegee. As can be observed within Figure 2B stage 1, the first layer is deposited, for example onto micron thick plastic, where the working and counter electrode have been formed with the corresponding connection legs. These are either cured within an oven or using UV light. Next the *pseudo*-Ag/AgCl reference is printed and again, cured (stage 2, Figure 2B). Last, the non-conducting ink (dielectric layer) is screen-printed which covers the connecting lengths (stage 3, Figure 2B) where again, it is cured. This produces the screen-printing electrodes which can be used "as is" or it can be modified further with bulk modified ink or using a nanomaterial via drop-casting. Note that screen-printing is versatile, where it can be used to print electrodes onto various substrates, predominately plastic, but other surfaces can be used, for example ceramic, neoprene, textiles, glass, skin and paper;[1–7] see reference[8] for an overview of the supporting material.

The downsides of screen-printing is the cost of the machine and running costs, and there is a need for screens, which define the electrochemical area and associated parts comprising the overall electrochemical sensing platform. For example, a new screen need to be designed, fabricated and this need replacing when the mesh has stretched, meaning that the working electrode size can change which is a contributing factor to batch-to-batch variation and printing quality (thickness of printed layer and uniformity of conductive material). Another aspect is the spillage/contamination of the working electrode by the ink/paste used to make your reference electrode–one needs to rigorously clean between each step (Figure 2). Environmental impact is often overlooked when researchers report the use of screen-printed electrodes. For example, waste generation is a matter of issue where the production process of screen-printed electrodes involves the use of solvents, screens, materials that can contribute to environmental waste; the disposable nature of screen-printed electrodes adds to the waste issue.

When fabricating screen-printed electrodes, one can make them on different substrate sizes ranging from A1 down to A5, but one needs to provide quality control to determine whether the screen-printed batch is useful (or not!) to proceed as the basis of screen-printed electrode platforms. The quality control of these systems can include: 1) a visual inspection for print quality; 2) in-process inspection checks such as the resistance measurement of the dried printed structure, image stretch and layer-to-layer registration measurements; 3) electrochemical examination (cyclic voltammetry) across printed card, row to row and through batch measuring peak current (I_p), peak potential (E_p), and the heterogeneous electron transfer rate constant (k^0); 4) microscopic measurement of the diameter and/or geometric area of the dried ink deposited upon the screen-printed electrode using a coordinate measuring instrument; 5) the measurement of deposition thickness via white light profilometry. A combination of the above[1–5] can be used to determine the quality of a batch of screen-printed electrodes.

Screen-printed electrodes have been reviewed for various applications, for example, carbon nanomaterials-based screen-printed electrodes for sensing applications,[32] biosensing,[33–36]

ChemElectroChem

Review
doi.org/10.1002/celc.202400370

Chemistry Europe
European Chemical
Societies Publishing

Figure 2. A: An overview of how screen-printed electrodes are fabricated, where the ink is screen-printed through being forced through a screen mesh. **B**: A summary of how each layer is composed in order to screen-print electrodes.

new directions in screen-printed electroanalytical sensors,[10] environmental monitoring,[14,22] food and drink safety,[13] heavy metals,[12,37] transitioning the laboratory in-to-the field,[9] pharmaceutical applications[38] and wearable sensors[39] to name just a few. In this review, we build upon previous reviews of screen-printed electrodes,[8–10,12–14,22,32–39] covering recent highlights of using screen-printed carbon electrodes used for electroanalysis and then turn to metallic and bulk modified electrodes, geometrically modified electrodes, electrode activation procedures and the physical connection length of screen-printed electrodes.

2. Screen-Printed Carbon Electrodes

Screen-printed carbon electrodes are the most utilised screen-printed sensing platforms which offer mass-producible, low-cost and highly reproducible electrochemical platforms, where graphite, carbon nanotubes[40–42] and graphene[43–46] are the most widely used allotropes of carbon. As mentioned above, the number of papers that report the use of screen-printed electrodes has substantial increased over the last decade. It would not be of any use to summarise the last 5 or 10 years within an endless table, but herein, we summarised some of the most promising approaches that report the use of screen-printed carbon electrodes within Table 1.

ChemElectroChem

Review
doi.org/10.1002/celc.202400370

Chemistry Europe
European Chemical
Societies Publishing

Table 1. A collection of the use of graphite screen-printed electrodes as the basis of electrochemical sensing platforms.

Modification	Analyte	Dynamic range	Limit of Detection	Matrix	Reference
MIP/Au NPs	Proline	1×10^{-16} – 0.01 M	9.18 aM	Cucumber seedlings	[49]
MIP	Hepatitis C	0.18–925 pM	8.5 fM	Human plasma	[48]
MIP	Irbesartan	20–220 nM	12 nM	Tap water	[47]
None	MDMA	0.005–1 mM	15 μM	Ecstasy street samples	[54]
Magnetic beads/Immunoassay	5-fluorouracil	5–100 ng/mL	1 ng/mL	Human serum	[63]
None	Quercetin and carbendazim simultaneously	0.1–1 μM	51.8 nM; 60 nM	Wine samples	[57]
None	Antimony (III)	1–910 μg/L	0.58 μg/L	Drinking water	[52]
None	Vitamin D_3	59.4 to 1651 μM	19.4 μM	Tablets	[53]
None	Selenium (IV)	10–1000 μg/L	4.9 μg/L	Drinking water	[51]
Bismuth film/ MWCNTs	Thallium (I)	10 nM–1 μM	2.8 nM	River water	[55]
Melanin nanoparticles	Chromium (IV)	0.1–2 μM	0.03 μM	Tap and lake water	[56]
Au NPs/MoO_3/ Chitosan/graphene	Carbohydrate antigen 19–9 (CA19-9); carcinoembryonic antigen (CEA)	0.0025–0.1 U mL^{-1} and 0.1–1.0 U mL^{-1} for CA19-9, and 0.001–0.01 ng mL^{-1} and 0.01–1.0 ng mL^{-1} for CEA	1.0 mU mL^{-1} CA19-9; 0.5 pg mL^{-1} CEA	Human blood serum	[64]
SiO_2/ZrO_2/ Cdot-N	Ceftriaxone	0.0078–40 μM	0.2 nM	Synthetic urine, urine, tap water	[50]
Tyr/PGA/CNF-IL	Tyramine	0.2–48 μM	91 nM	Malt drink and pickle juice samples	[65]
NiO/carbon black	5-hydroxymethylfurfural	0.5–10.0 mg kg^{-1}	5.4 mg kg^{-1}	Honey	[61]
GO/PHB/Antibody	SARS-CoV-2-(N-protein)	50 pg/mL–25 ng/mL		Saliva, serum and nasal swab	[66]
None	Nicotine	10–800 μM	1.7 μM	Tabacco leaves	[58]
None	5-Methoxy-N-methyl-N-isopropyltryptamine	0.05–30 μM	0.015 μM	Seized samples	[67]
$La_2Sn_2O_7$	Ractopamine	0.01–501 μM	0.86 nM	Pork and sausage	[59]
Boron carbon nitride	Tryptophan	1–400 μM	36 nM	Urine and egg white	[68]
Domoic and okadaic acids	Carbon black/Antibodies	4–72 ng/mL; 0.27–3.3 ng/mL	1.7 ng/mL; 0.18 ng/mL	Shellfish	[69]
Formaldehyde	Egg albumin with ZnO	1–5 μM	6.2 nM	Urine	[60]
Interleukin-6	Biochar/antibody	26–125 and 30–138 pg/mL	4.8 pg/mL	Human blood	[70]
Ag NPs	Arsenic (V)	1.9–25 μg/L	0.6 μg/L	Tap water	[62]
Metronidazole	GO/C_{60}	0.25–34 μM	0.21 μM	Urine and synthetic serum	[71]

Key: Ag NPs: silver nanoparticles; Au NPs: gold nanoparticles; Cdot-N: nitrogen-doped carbon quantum dots; GO: graphene oxide; IL: 1-butyl-3-methylimidazolium hexafluorophosphate; MIP: molecular imprinted polymer; MWCNTs: multiwalled carbon nanotubes; PGA: poly(glutamic acid); PHB: polyxydroxybutyrate; Tyr: tyrosinase.

2.1. Molecular Imprinted Polymers-modified Screen-Printed Electrodes

For example, the addition of molecular imprinted polymers (MIPs) to the surface of a screen-printed carbon electrode for the production of low-cost sensors as the basis of a sensor for irbesartan, a medicine used in patients with hypertension and those with type 2 diabetes mellitus and nephropathy.[47] Using commercially available screen-printed carbon electrodes, the authors functionalised the electrode surface using a prepoly-

ChemElectroChem

Review
doi.org/10.1002/celc.202400370

Chemistry Europe
European Chemical
Societies Publishing

meric solution which is obtained by mixing irbesartan, methyacrylic acid, and ethylene glycol dimethacrylate into ethanol in the molar ratio of 1:4:10. Next, 2,2-azobisisobutyronitrile was added and is sonicated until obtaining a limpid solution. Using screen-printed electrodes, they drop-coated the surface where thermal polymerisation was carried out in a thermostatic oven at 60 °C overnight.[47] This sensor is shown that a linear range of 20–220 nM with a limit of detection (LoD) of 12 nM is possible.[47] Such an approach allow low cost, but yet mass-producible sensors based upon screen-printed electrodes. Note that the development of MIPs tailored to screen-printed electrochemical platforms has accelerated the shift from bulky conventional techniques to economical and rapid-sensing devices for in-field analyses.[47] MIPs have also been developed for Hepatitis C, which reported impressive linear range of 0.18–925 pM with a limit of detection (LoD) of 8.5 fM,[48] and proline, an important amino acid which is crucial to plant growth and development.[49] The authors report an impressive linear range and limit of detection (LoD) of 1×10^{-16}–0.01 M and 9.18 aM respectively; see Figure 2A.[49] The screen-printed graphite electrode is decorated with gold nanoparticles via electrochemical deposition, then thionine was electrochemically polymerised. Next, this modified electrode is immersed into proline and pyrrole where the MIP is formed via cyclic voltammetry, after which the embedded proline is extracted revealing a MIP ready for sensing. The authors show their sensor can be used to measuring free proline in the leaves of living cucumber seedlings under salt stress and has the benefit of being simple, rapid and portable, which make it suitable for on-site and in-situ detection.[49] The authors note that the measurement of proline sensors have been developed using glassy carbon and gold electrodes where the volume of these are too large for in-vivo detection as the leaves of plants are flat and thin and it is difficult to find suitable electrode to insert into them for in-vivo testing and opted to use a flat screen-printed electrodes.[49] These examples show how the simple inclusion of MIPs as recognition elements alongside screen-printed electrodes can create reliable and sensitive sensing devices while being economical and easily mass produced.
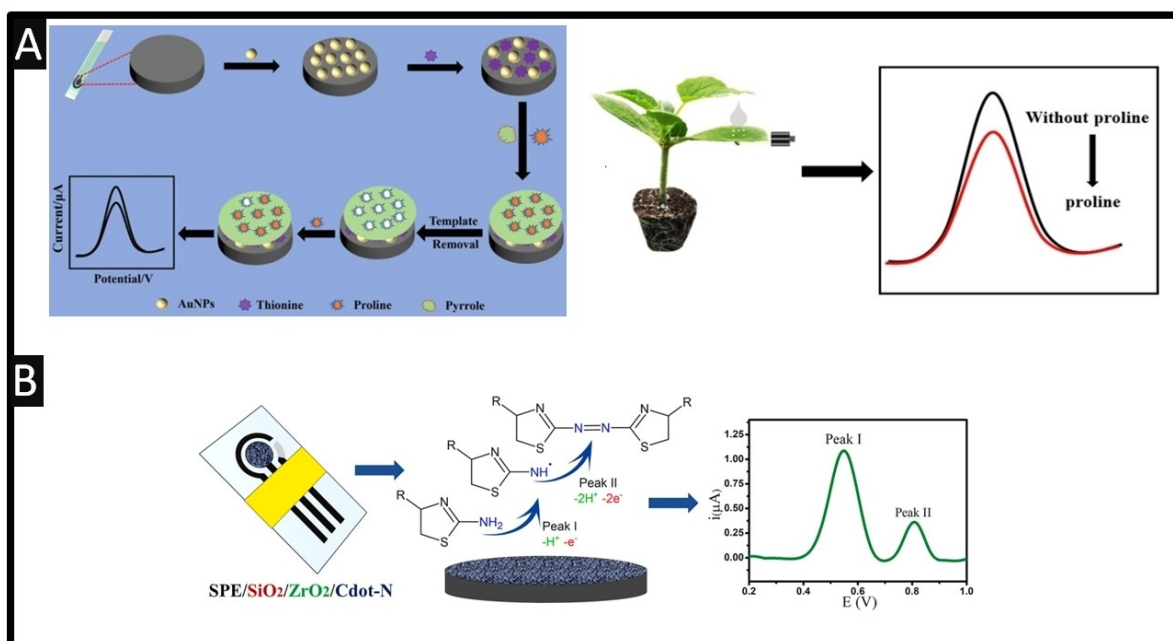
2.2. Non-Modified Screen-Printed Electrodes

As summarised within Table 1, many of the electrochemical screen-printed platforms are used "as is", for example for the detection of selenium (IV) and antimony (III),[51,52] where both exhibit LoDs lower that the levels set by the United States Environmental Protection Agency. These show evidence toward use as screening tools within drinking water samples, as well as for the sensing of vitamin D_3[53] and MDMA.[54] More work has been reported using a bismuth film deposited upon a multi-walled carbon nanotubes coated screen-printed graphite electrode for the sensing of thallium (I) providing a LoD of 2.8 nM, which was shown to be successful in measuring thallium (I) within river water.[55] Additionally, there are reports of melanin nanoparticle modified screen-printed graphite electrodes for the detection of chromium (IV).[56] In this work the modified

screen-printed graphite electrodes produced a wide linear range of 0.1–5 μM, a sensitivity of 0.52 μA μM^{-1}, and a LoD of 0.1 μM, and was successfully applied to the determination of Cr (IV) in tap and lake water samples. Other work has reported on the simultaneous determination of quercetin and carbendazim within wine samples. Quercetin is a polyphenol flavonoid found in teas and grapes, where its concentration depends on the grape variety, harvest, soil type, geographical origin and wine-making techniques used. While carbendazim is a benzimidazole fungicide used to eradicate pathogens or fungal diseases in vegetables and fruits.[57]

A dual mode for the in-situ detection of nicotine has been reported where a linear range of 10–800 μM and a LoD of 1.7 μM.[58] This approach used paracetamol as an internal standard which was shown to be successful in the determination of nicotine within tobacco leaves where the sensor is clamped onto the leaves. Importantly, this was successfully validated against high performance liquid chromatography. Other work has reported the electrochemical oxidation of ceftriaxone, an antibiotic, through the use of a screen-printed graphite electrode decorated with nitrogen-doped carbon quantum dots, silicon oxide and zirconium oxide;[50] see Figure 3B. Two oxidation peaks were observed, with a possible reaction postulated to be the electrochemical oxidation of ceftriaxone occurring at the aminothiazole substituent group, characteristic of the cephalosporins class. In this way the amino group of this substituent oxidizes with the loss of one hydrogen cation and one electron forming an imino radical (peak I) which subsequently forms dimer molecules. The second peak (peak II) is the oxidation at the binding site where the dimer molecules were formed, which involves the release of two electrons and two hydrogen cations, enabling the formation of a double bond.[50] This sensor was able to detect ceftriaxone over the range of 0.0078–20 μM with a LoD of 0.2 nM using square-wave voltammetry. Their sensor was shown to measure ceftriaxone within synthetic urine, human urine and tap water with recoveries of 95–105%; this work has potential to provide a rapid, cost-effective, disposable sensor for ceftriaxone.

2.3. Metal-Oxide/Nanoparticles Modified Screen-Printed Electrodes

Of interest is the use of a $La_2Sn_2O_7$ modified screen-printed graphite electrodes used in the sensing of ractopamine. Ractopamine is used as a feed additive to induce animal growth stimulant effects, and it can be accumulated within the liver and various parts of the body which can contribute to cardiac palpitations, tachycardia, malignant tumours and cardiovascular diseases. As such, there needs to be rapid sensors for the determination of ractopamine within meat products for screening.[59] The authors prepared their $La_2Sn_2O_7$ through the use of lanthanum(III) nitrate hexahydrate, tin(II) chloride and CTAB added to water which are mixed for 2 hrs, following these are added to a Teflon autoclave which is kept at 160 °C for 16 hrs. Next, the precipitate, $LaSn(OH)_6$ is centrifuged with water and ethanol and then is calcined at 650 °C for 3 hr leading to

ChemElectroChem

Review
doi.org/10.1002/celc.202400370

Chemistry
Europe
European Chemical
Societies Publishing

Figure 3. A: The use of MIPs being formed upon a screen-printed graphite electrodes that can be used for the measurement of proline. Reprinted with permission under a Creative Commons attribution-type BY from reference.[49] B: An overview of the sensing of ceftriaxone. Figure reproduced from reference.[50] Copyright 2014 Elsevier.

the formation of $La_2Sn_2O_7$ nanoparticles (~83 nm in diameter). These are then drop-cast onto the screen-printed graphite electrodes where the authors report a liner range of 0.01–501 μM and a LoD of 0.86 nM for the determination of ractopamine; the benefit of $La_2Sn_2O_7$ is the rapid rate of reaction kinetics favoured by the active penetration of electrolyte ions into the surface of the electrode.[59] The authors validated their sensor within spiked pork and sausage meat samples which it is compared to HPLC reporting close agreement between the two methodologies providing a useful electrochemical sensing platform for the measurement of ractopamine.

Padmalaya and co-workers[60] report on the sensing of formaldehyde, a hazardous pollutant, using egg albumin with ZnO rice structure which is fabricated via a wet chemical technique. The authors compared their sensing with other reports for sensing of formaldehyde where the use of egg albumin with ZnO rice structure improves the adsorption of formaldehyde enhanced by protein (egg white). The sensor reports a LoD of 6.2 nM where interferents were studied were negligible effects were reported on the sensing of formaldehyde in the presence of ammonia, cadmium and lead where the authors comment on the use of screen-printed graphite electrodes modified with egg albumin and ZnO rice structure giving rise to an on-spot sensor which has high sensitivity, reusability, simplicity, a wide operational range and of course, low cost.[60]

Through the use of square-wave voltammetry and a nickel oxide and carbon black modified screen-printed graphite electrode the sensing of 5-hydroxymethylfurfural in honey samples has been reported.[61] 5-hydroxymethylfurfural is of interest as levels in honey can provide adverse effects from

high doses. Consequently, the Codex Alimentarius Standard Commission and the European Union (EU) have established specific maximum residue limits for 5-hydroxymethylfurfural in honey from tropical countries, which should not exceed 80 and 40 $mg\,kg^{-1}$, respectively. Hence there is a requirement to quantify 5-hydroxymethylfurfural. The authors prepared their nickel oxide by dissolving the metal salt into water with sodium hydroxide which was then transfer into a Teflon autoclave to heat at 90 °C for 8 hrs. This was then added to carbon black which was then drop casted onto the surface of the electrodes. The sensor reports the linear range and LoD of 0.5–10.0 $mg\,kg^{-1}$ and 5.4 $mg\,kg^{-1}$ respectively. Interestingly, honey is dissolved into water, homogenized and then is ready to use via a pH change. The authors compared their analysis against HPLC which provided a high degree of agreement; the authors note that their approach is simple and convenient making it suitable for the sensing of 5-hydroxymethylfurfural within honey.[61] Work by Torres-Rivero et al.[62] have explored the use of silver nanoseeds (16 nm) against silver nanoprisms (14 nm) for the sensing for arsenic (V) supported upon a screen-printed graphite electrode. In the case of the silver nanoseeds, they exhibited a linear range of 1.9–25 μg/L with a LoD of 0.6 μg/L while in the case of silver nanoprisms, a linear response of 4–25 μg/L with a LoD of 1.2 μg/L, the answer to why different results are observed are likely to the amount of silver residing on the electrode surface. The authors compared their sensor directly with the sensing of arsenic (V) with spiked tap water with ICP-MS which achieved statistically comparable results.

Cotchim and co-workers[64] report dual screen-printed graphite electrodes for the simultaneous detection of carbohydrate antigen 19–9 (CA19-9) and carcinoembryonic antigen

ChemElectroChem

Review

doi.org/10.1002/celc.202400370

Chemistry Europe
European Chemical
Societies Publishing

(CEA) as biomarkers of cholangiocarcinoma, which is a primary malignancy that arises from bile duct epithelial cells. The authors used gold nanoparticles supported onto MoO_3 with chitosan as a stabilising agent, all supported on porous graphene. As shown within Figure 4A, the electrodes are modified with the corresponding antibodies which are directly adsorbed onto gold nanoparticles via hydrophobic, hydrophilic, and electrostatic interactions between the antibodies and the gold nanoparticles surfaces which allowed them to report linear ranges of 0.0025–0.1 U mL^{-1} and 0.1–1.0 U mL^{-1} for CA19-9, and 0.001–0.01 ng mL^{-1} and 0.01–1.0 ng mL^{-1} for CEA with LoD of 1.0 mU mL^{-1} for CA19-9 and 0.5 pg mL^{-1} for CEA. The authors demonstrated their immunosensor with the measurement of CA19-9 and CEA within spiked human blood serum reporting recoveries from 88–99.3% with low RSDs. This work provides a hope that this alternative method can replace clinical diagnosis providing a sensitivity yet rapid onsite immunosensor; further work is required to expand the measurement of the electroanalytical based immunosensor and to compare it directly with clinical diagnosis.

The use of screen-printed graphite electrodes is used for the sensing of 5-fluorouracil since it remains one of the most effective anticancer drugs for colorectal cancer. As shown within Figure 4B,63 the 5-fluorouracil competed with 5-fluorouracil-BSA covalently immobilized on carboxylated magnetic beads (HOOC-MBs; 2.8 μm diameter) for the recognition sites of a limited amount of a 5-fluorouracil -selective detection anti-

body (DAb) labelled with a horseradish peroxidase tagged secondary antibody (HRP-antimIgG). This was used to perform amperometry with the hydrogen peroxide–hydroquinone electrochemical based system which gives rise to the electroanalytical signal.[63] Using carboxylated magnetic beads, carboxyl groups are activated within a N-(3-dimethyl-aminopropyl)-N′-ethyl-carbodiimide/N-hydroxysulfosuccinimide solution for 35 mins. After which, these are washed twice and are incubated for 15 mins with 5-fluorouracil-BSA for covalent immobilisation. The 5-fluorouracil-BSA- carboxylated magnetic beads are washed twice and the uncreated groups upon the carboxylated magnetic beads are deactivated by incubation for 60 min within 0.1 M ethanolamine solution. Next, the fluorouracil-BSA- carboxylated magnetic beads are incubated for 30 min in a mixed solution containing fluorouracil-BSA (or the sample to analyze) and a diluted DAb solution. DAb-5-fluorouracil-BSA-carboxylated magnetic beads are washed then incubated for 30 min in a solution containing HRP-antimIgG antibody. After two washing steps with PBS, the resulting magnetic immunoconjugates, HRP-antimIgG- DAb-5-fluorouracil-BSA- carboxylated magnetic beads are resuspended in a phosphate buffer. This is drop cased onto the screen-printed electrode surface where amperometric measurements are performed by holding the potential at −0.2 V (Ag pseudo-reference electrode) which immunoassay gave a linear rage of 5–100 ng/mL with a LoD of 1 ng/mL and was shown as a proof-of-concept to be successful
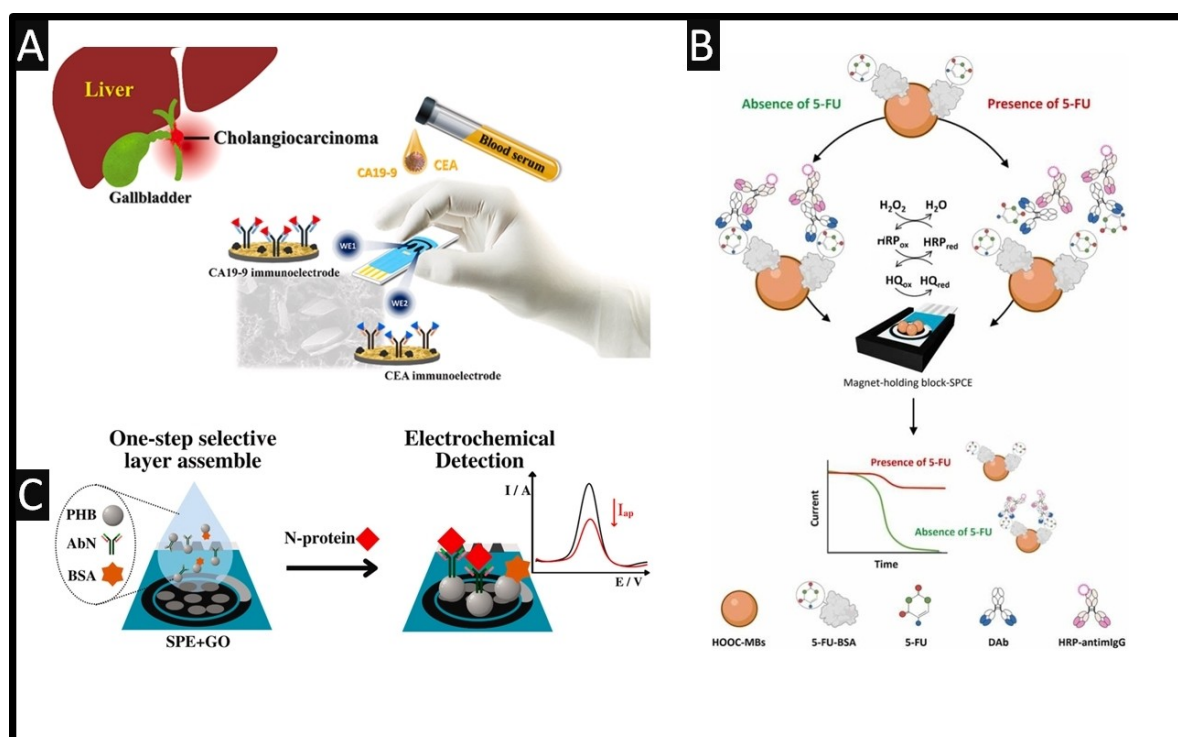
Figure 4. A. Summary of the electrochemical immunosensor for cholangiocarcinoma. Figure reproduced from reference.[64] Copyright 2024 Elsevier. **B**: Schematic diagram of the proposed 5-fluorouracil immunoassay strategy taking advantage of an indirect competitive assay performed on the surface of MBs and amperometric transduction using screen-printed graphite electrodes. Figure reproduced from reference.[63] Copyright 2024 Elsevier. **C**: An overview of the use of polyhydroxybutyrate (PHB) alongside graphene oxide for anchoring specific antibodies against SARS-CoV-2 nucleocapsid protein (AbN) for the detection of virus antigen (N-protein) in three different matrixes: saliva, serum, and nasal swab. Figure reproduced from reference.[66] Copyright 2023 Elsevier.

ChemElectroChem

Review
doi.org/10.1002/celc.202400370

Chemistry
Europe
European Chemical
Societies Publishing

in the measurement of 5-fluorouracil within spiked human serum.

As summarised within Figure 4C, an overview of the use of polyhydroxybutyrate (PHB) using graphene oxide for anchoring specific antibodies against SARS-CoV-2 nucleocapsid protein (AbN) for the detection of virus antigen (N-protein) have been reported in three different matrixes of saliva, serum, and nasal swab.[66] Using commercially available screen-printed electrodes, the authors electrodeposited graphene oxide which involves graphene oxide being drop-casted onto the electrochemical surface, using cyclic voltammetry where the potential is scanned form −1.4 V to 0.0 V (50 mV/s) up to 10 cycles which promotes partial reduction of oxygenated groups in graphene oxide forming electrochemical reduced graphene oxide. In essence, increasing the number of active sites allows adsorption of the PHB protein binding agent. The sensor is fabricated by drop casting PHD onto the electrode surface, oven-dried where AbN are also dropped on the electrode surface, again oven dried. Next PHD residual active sites that did not bind to AbN are blocked by adding using bovine serum albumin. The device is Then, the device was applied for the detection step, in which a solution containing N-protein antigens was incubated on the electrode. After this step, once again a decrease in the probe redox process was observed, due to the formation of the antibody-antigen immunocomplex on the electrode surface. The sensor is applied for the detection step, where a solution containing N-protein antigens was incubated on the electrode which results in the decrease of the probe redox process due to the formation of the antibody-antigen immunocomplex on the electrode surface (see Figure 4C).[66] This sensor reports a LoD of 50 pg/mL and a linear range from 50 pg/mL to 25 ng/mL. Using screen-printed electrodes in the first instance, allows the authors to consider commercialisation sooner rather than later, since making the sensor work on a carbon solid electrode will need to be reengineered onto screen-printed electrodes adding more costs, time and hinder commercialisation.

3. Screen-Printed Metallic Electrodes

Screen-printed metallic electrodes are less common that screen-printed graphite electrodes mainly due to the high, and fluctuating costs which change as the price of the metal increases/decreases. Table 2 summarises the use of screen-printed metallic electrodes and covers the use of polycrystalline gold, silver, palladium and copper. One can observed that gold electrodes have been numerously used. A pertinent question is: Why is gold chosen over platinum, silver, palladium and copper? Gold is a popular and frequently used electrode material due to the following benefits: fast electron transfer kinetics, high conductivity, environmentally friendly character, and it has a potential window with a comparatively wide anodic range. Other factors include the market cost of the materials and scarcity.

The use of screen-printed metallic electrodes is summarised within Table 2 which shows that researchers either use them "as is" or they modify them. Significant amounts of work have

reported the use of screen-printed metallic electrodes for the sensing of "heavy metals". Note that this terminology is meaningless, but rather we should employ this by metal, metalloid according to the case, or by potentially toxic element or trace metals.[93] We can observe from inspection of Table 2 that chromium (III) and (V), as well as arsenic (II) have been reported using gold electrode platforms reporting competitive LoDs.[72,74,75] Interestingly, reports on the ultrasensitive voltammetric determination of the antipsychotic drug thioridazine have reported a linear range of 10 pM–20 nM with an impressive LoD of 2.9 pM using a gold screen-printed electrode which resides in the form of gold oxide.[73] Thioridazine is used in the treatment of schizophrenia where it is administered to patients who do not respond sufficiently to treatment with other antipsychotics. Thioridazine administered at high levels can result in deadly neuroleptic malignant syndrome exerting its effect through central dopamine-blocking, minor anticholinergic activities and adrenergic-blocking.[73] The authors demonstrated their sensor can be used in the determination of thioridazine in spiked human serum and treated wastewater which reported recoveries of 98.5–102.5%. It is reported that the maximum concentration in blood of patients taking thioridazine are in the range of 0.3 to 1.3 μM where the authors sensor can be used in the measurement of thioridazine.[73] These results suggest that the use of metallic screen-printed electrode based sensor is commercially available avoiding time-consuming process of preparing the sensor as well as the reagents needed for it.[73] Further work should be directed to the comparison of their sensor against gold laboratory approaches and within real blood samples.

Other work has reported the use of a silver screen-printed electrodes towards cystine detection within urine samples and pharmaceutical tablets.[92] The measurement of cystine within urine can signal the presence of cystinuria, a rare genetic disorder where the kidneys excrete excessive cystine into urine, causing abnormal excretion of cystine and can potential lead to the formation of cystine stones.[92] The authors demonstrated the use of the silver screen-printed electrodes against that of a graphite screen-printed electrode, where the latter did not show any electrochemical reduction towards cystine, but in the case of the former, a large and quantifiable signal is reported at ~−0.47 V. Both were recorded within 1 M hydrochloric acid solution, and it is proposed that the silver surface provides adsorption sites for cysteine, whereas the graphite does not. Using amperometry, the authors reported a linear range and a LoD of 2.4–48 mg/dL and 0.65 mg/dL respectively. Furthermore, the authors assess potential interference where using a solution of 24 mg/dL of cysteine, the author separately added in urea (6.06–30.3 g/L), creatinine (25–390 mg/dL), and vitamin C (0.3–1.2 mg/L), with no effect on the sensing of cystine.[92] The author demonstrated their sensor towards spiked cystine in urine sample is viable where they report recoveries of 91–109%. The urine samples were provided by volunteers where 10 mL of midstream urine was collected and mixed with 6 M HCl at a volume ratio of 5:1, along with 6.06 g/L urea and 130 mg/dL creatinine. The mixture was then subjected to electrochemical reduction at −0.6 V for a duration of 10 s and

ChemElectroChem

Review

doi.org/10.1002/celc.202400370

Chemistry
Europe
European Chemical
Societies Publishing

Table 2. A selection of the use of metallic macrodisc screen-printed electrode used as the basis of electrochemical sensing platforms.

| Electrode material	Analyte	Modification	Dynamic range	Limit of Detection	Reference
Gold	Chromium (III) and (VI)	–	100–1600 μM; 100–1600 μM	38.8 μM;4.4 μM	[72]
Gold	Thioridazine	–	10 pM–20 nM	2.9 pM	[73]
Gold	Chromium (VI)	–	10–50 μM	2.6 μM	[74]
Gold	Arsenic (III)	–	0–20 μg/L	0.8 μg/L	[75]
Gold	Monosaccharides (glucose and fructose)	Schiff base Ni complex	36–130 μM; 48–130 μM	36 μM; 48 μM	[76]
Gold	Ochratoxin A and Aflatoxin M1	3-mercaptopropionic acid/EDC/NHS/AB	0.05–136 ng/mL; 0.04–205 ng/mL	15 ng/mL; 37 pg/mL	[77]
Gold	HER2 protein	Aptamer/MCH/HDT	1 pg/mL–1 μg/mL	172 pg/mL	[78]
Gold	Vaspin	Coccolith shell/aptamer	2–16 nM	298 pM	[79]
Gold	Thiocholine	Cysteamine/glutaraldehyde/AChE	–	40 μg/L	[80]
Gold	Guanine and adenine	MIP	5–50 nM, 50–500 nM; 5–50 nM, 5–700 nM	0.37 nM; 1.25 nM	[81]
Gold	Cadmium (II) and lead (II) ions	GO/ruthenium (II) bipyridine complex/Nafion®	50–350 μg/L	4.2 μg/L; μg/L	[82]
Gold	Uric acid	Au/KOH/AuNPs/SAM/UOX	50–1000 μM	4.4 μM	[83]
Gold	Bungarus candidus	Antibody	0.1–0.4 mg/mL	4.3 μg/L	[84]
Gold and platinum	Hydrogen peroxide	Prussian Blue	5–50 μM	-	[85]
Platinum	Hydrazine	–	50–500 μM	0.15 μM	[86]
Platinum	Hydrogen peroxide	–	100–1000 μM	0.24 μM	[86]
Palladium	Formaldehyde, hydrazine and protons	–	2.5–6.5 mM; 200–1000 μM; 100–1000 μM	1.6 mM; 4.0 μM; 41.5 μM	[87]
Copper	Sulfide	–	50–1000 μM	41 μM	[88]
Silver	L-lactic acid	Mercury	40–500 μM	12 μM	[89]
Silver	Nitrate	Copper nanoparticles	0.05–5 mM	0.20 nM	[90]
Silver	Chlorpyrifos	11-MUA/EDC/NHS/aptamer	1–10^5 ng/mL	0.097 ng/mL	[91]
Silver	Cystine	–	2.4–48 mg/dL	0.65 mg/dL	[92]

Key: AB: antibody; AChE : acetylcholinesterase; Au: gold; GO: graphene oxide; HDT: 1,6-hexanethiol; MCH: 1-mercapto-6-hexanol; MIP: molecularly imprinted polymer; 11-MUA: 11-mercaptoundecanoic acid; KOH: potassium hydroxide; SAM: functionalized self-assembled monolayer; UOX: uric acid oxidase.

then the sample is spiked with cystine and determined via the standard addition protocol. This system shows the unique way in which metallic electrodes can be advantageous for specific applications, not only due to their improved conductivity. The use of copper screen-printed electrodes have be utilised for sulfide,[88] where their approach overcomes the poor performance of graphite screen-printed electrodes. Such an approach avoids the use of pre-treatment step using electrochemically deposited copper nanoparticles prior to use. The authors demonstrated their sensor can be used in the measurement of sulfide over the range of 50–1000 μM where a LoD of 41 μM is possible using linear sweep voltammetry. This proof-of-concept approach is shown to be useful for the measurement of sulfide within spiked tap water where recoveries of 99.4–102.1 % are reported.[86] Through characterisation of metallic screen-printed electrodes, which clearly is never already provided, the copper resides as a copper oxide (copper II oxide) nanoparticle formulation which promotes the electrochemical oxidation of sulfide. It can within Table 2, that researchers have modified their metallic screen-printed electrochemical platforms, for

example, the covalent attachment to a self-assembled monolayer of MPA (3-mercaptopropionic acid) on the gold surface is used where the application of EDC/NHS to convert the terminal carboxylic groups into an active NHS ester; see Figure 5A.[77] This approach allowed the authors to prepare a competitive immunoassay format, allowing the authors to measure Ochratoxin A in red wine and Aflatoxin M1 within milk giving a LoD of 15 ng/mL and 37 pg/mL respectively.[77] Such an approach overcomes the use of taking a graphite screen-printed electrode decorated with gold nanoparticles, where the stability of the sensor is based upon how stable (attached) the gold nanoparticles are.

Other work has used gold bulk modified screen-printed electrodes to form an immunoassay sensor for the detection of the tumour marker for breast cancer, Human Epidermal Growth Factor Receptor 2 (HER2).[78] As shown within Figure 5B, a mixed self-assembled monolayer with thiolated aptamer and a ternary self-assembled monolayer with aptamer, 1,6-hexanethiol (HDT) and 1-mercapto-6-hexanol (MCH) were prepared. Using EIS, the authors showed that the sensor can measure HER2 protein over
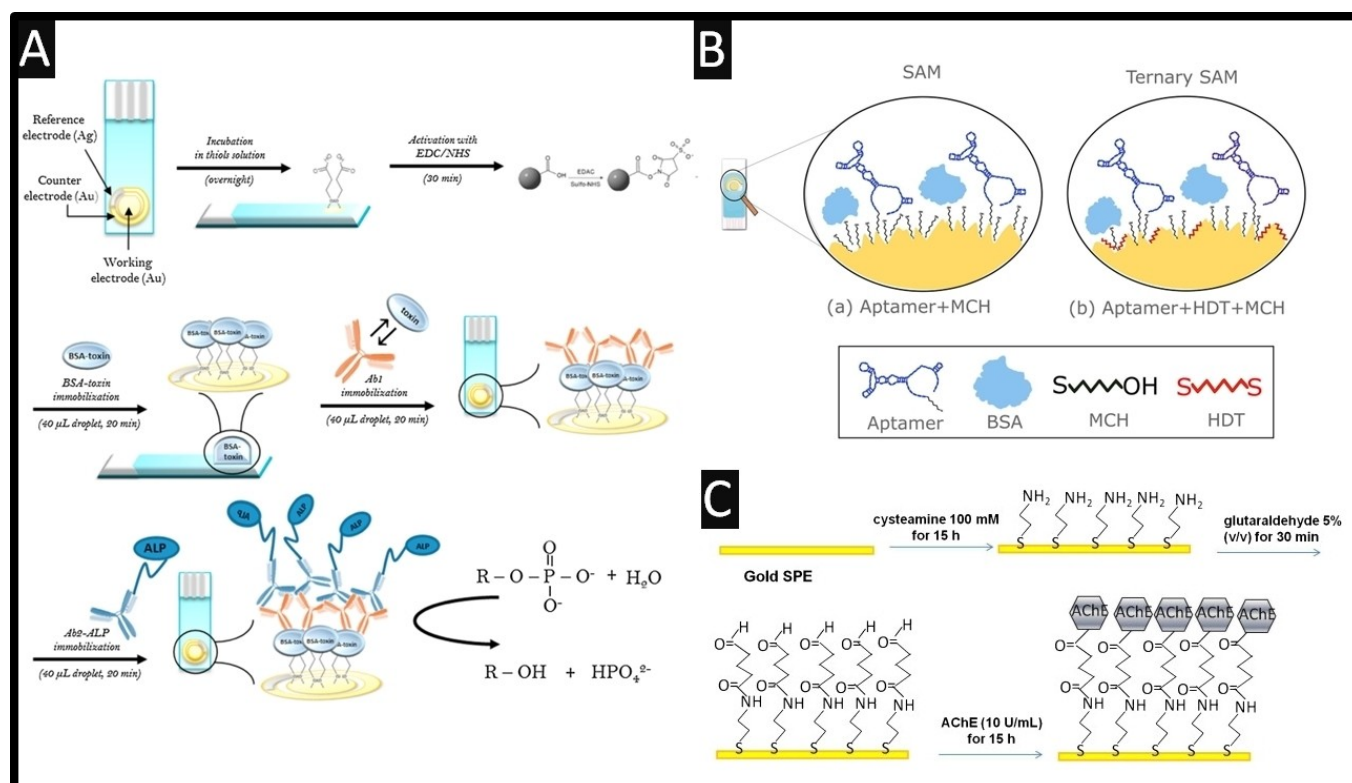
Figure 5. A: A schematic image of the preparation of the biosensor for toxin detection utilizing a gold bulk modified screen-printed electrode hosting a competitive immunoassay format. Figure reproduced from reference.[77] Copyright 2017 Elsevier. **B**: In (a) SPE modified with DNA Aptamer and MCH to form a self-assembled monolayer (SAM). In (b) SPE modified with DNA Aptamer, MCH and HDT to form a ternary SAM. The HDT can adopt a vertical or horizontal configuration, blocking the remaining spaces on the irregular surface. The molecules were not drawn to scale. Figure reproduced from reference.[78] Copyright 2021 Elsevier. **C**: An overview of the assembling of the AChE biosensor. Figure reproduced from reference.[80] Copyright 2013 Elsevier.

the range of 1 pg/mL–1 μg/mL and a LoD of 172 pg/mL within undiluted human serum. This work provides a strategy to measure a breast cancer marker and could be a promising tool for point-of-care detection and application. Other approaches use the metallic surface to be used for the physical adsorption of moieties, for example, as shown within Figure 5C, cysteamine, is applied after which glutaraldehyde and then with acetylcholinesterase.[80] This sensor gave rise to competitive LoD providing the basis of insecticide sensing.
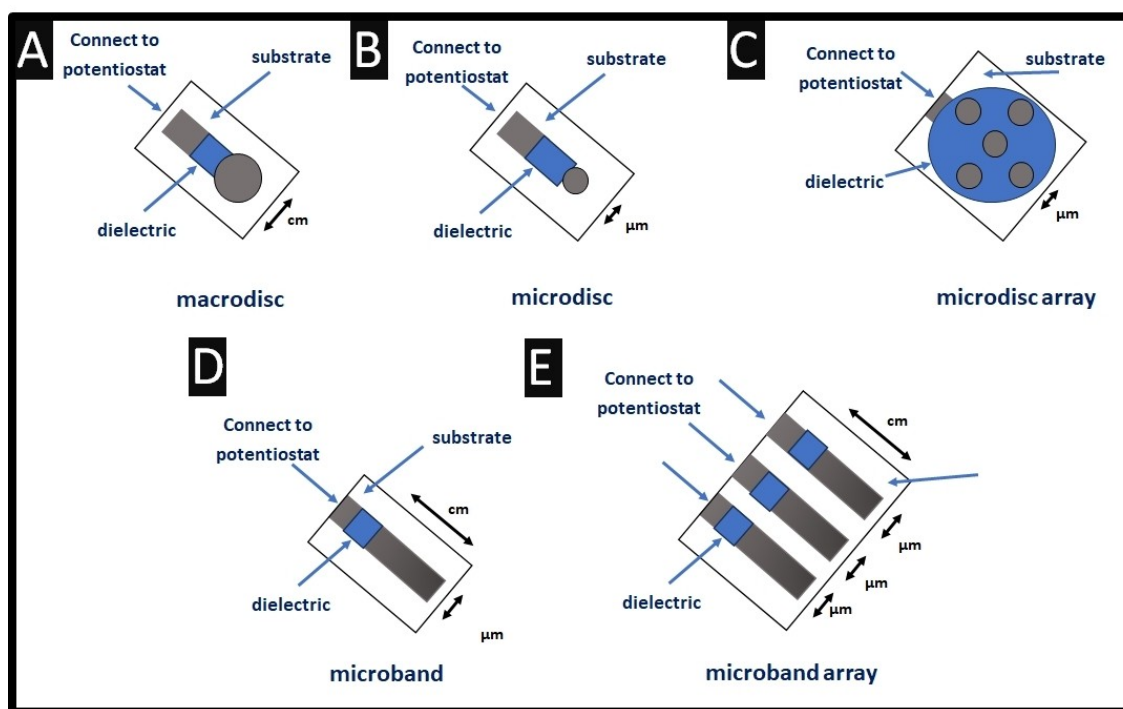
In summary, we can observe the range and diversity of the use of metallic screen-printed electrodes where the approach can use a pre-step prior to use via electrochemically decorated or drop-casting with metallic nanoparticles. Furthermore, authors make their metallic screen-printed electrodes and report their use straight away, where we note the oxide context of the metal is hardly reported; further work should consider this aspect on their sensor performance. Next, we turn to explore the use of screen-printed electrodes in terms of changing their size from macrodisc down to microdisc electrodes and the use of microbands and their associated arrays; please see Scheme 1 which summaries the geometry between each.

4. Screen-Printed Electrode Macro/Micro Arrays

4.1. Screen-Printed Electrode Macro Arrays

A multianalyte commercially available biosensor array for simultaneous and cross-talk free determination of the metabolites L-lactate, D-lactate, ethanol, and formate has been reported by Pilas and co-workers.[94] The sensor, as shown within Figure 6A, is composed of 4 working carbon electrodes sharing a common counter and reference electrode where the working electrodes comprise of 2.95 mm diameter. The sensor involves the use of graphene oxide after which cofactors are added and finally with the enzymes complete the sensors. The electrode surface was electrochemically activated at $+1.4$ V for 240 s in 100 mM KCl. Next, graphene oxide is mixed with the cofactors NAD^+, potassium ferricyanide and Nafion® which is drop-cast on the electrode surface and air-dried at room temperature. The electrode surface are then modified with the enzymes (1.5 U L-lactate dehydrogenase from *Bacillus stearothermophilus* and 6.0 U diaphorase from *Clostridium kluyveri*). Finally, cellulose acetate are drop-coated on top of the enzyme membrane. The multianalyte biosensor array for the simultaneous measurement of L-lactate, D-lactate, formate, and ethanol was realized by immobilizing a different dehydrogenase on one of the four working electrodes (WEs). The enzyme loading of the D-lactate and formate electrodes is as described above where each 1.5 U

ChemElectroChem

Review

doi.org/10.1002/celc.202400370

**Chemistry
Europe**
European Chemical
Societies Publishing

Scheme 1. An overview of the geometries of macroelectrodes (A), microelectrodes (B), microelectrode array (C), microband (D) and a microband (E) array.
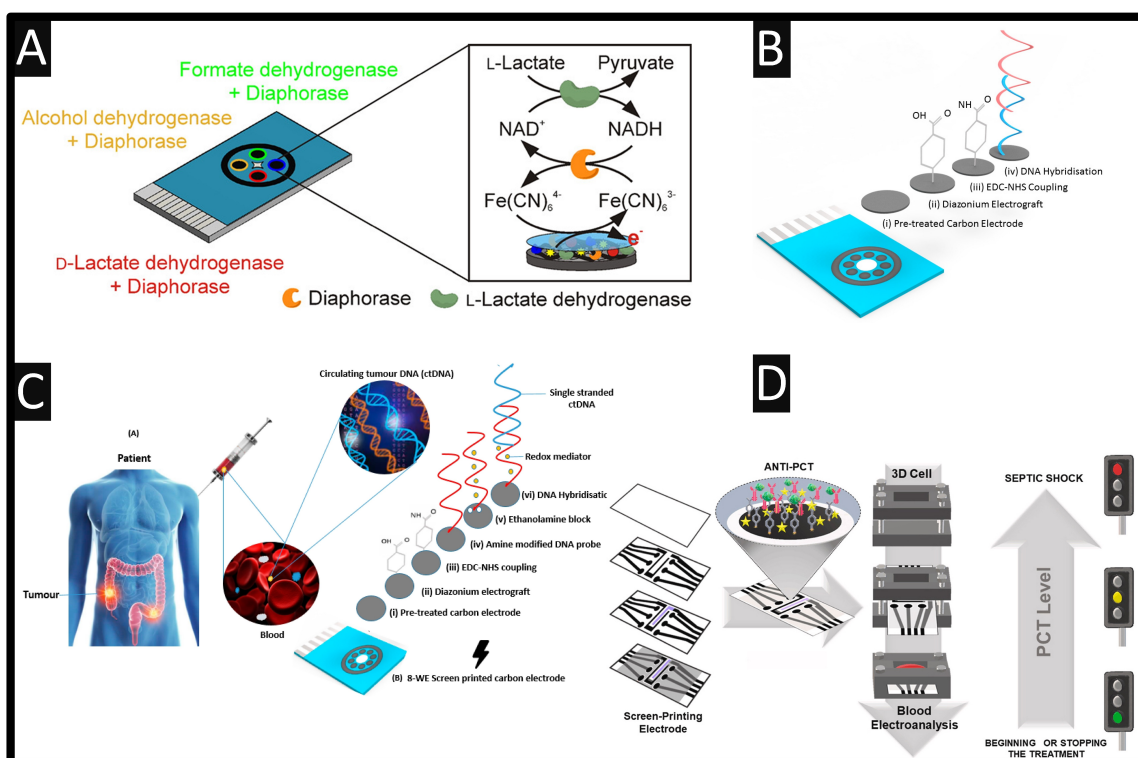

Figure 6. A: Schematic illustration of the multianalyte screen-printed carbon biosensor array. Figure reproduced from reference.[94] Copyright 2019 The American Chemical Society. **B**: Schematic illustration of a circulating tumor DNA sensor. Reprinted with permission under a Creative Commons attribution-type BY from reference.[95] **C**: An overview of the innovative in the development for a DNA sensor for the measurement of KRAS G12D and G13D point mutations in different tumour types. Reprinted with permission under a Creative Commons attribution-type BY from reference.[96] **D**: An overview of the design and facile production of screen-printed arrays (SPAs) for the internally validated determination of raised levels of serum procalcitonin (PCT). Reprinted with permission under a Creative Commons attribution-type BY from reference.[97]

ChemElectroChem

Review
doi.org/10.1002/celc.202400370

Chemistry Europe
European Chemical
Societies Publishing

of D-lactate dehydrogenase and cellulose acetate, respectively used. For the ethanol electrode, a dehydrogenase loading of 16 U alcohol dehydrogenase was used. Each sensor measured L-lactate, D-lactate, ethanol, and formate over the linear ranges of: 0.25–4.0, 0.25–4.0, 0.05–2.0 and 0.25–4.0 mM respectively which has a future in the monitoring of fermentation processes.[94] The design of this electrode has been extended for the DNA functionalisation and DNA target binding for circulating tumours; see Figure 6B for an overview of how the sensor was fabricated.[95] Work by Attoye et. al report a biosensor that utilises a KRAS G12D and G13D DNA oligonucleotide probe modified sensor array and can measure and detect mutant KRAS amplicons. This could form the basis of a system for the accurate detection of ctDNA in patient samples and monitoring of patient response during treatment; see Figure 6C.[96] This sensor is comprised of eight carbon electrodes, each 2.95 mm diameter. The working electrodes are prepared by applying a pre-treatment method by applying $+1.4$ V for 1 M in a 0.5 acetate buffer solution. Next, sodium nitrite and 4-amino-benzoic acid are prepared in 0.5 M HCl, stirred for 5 min at room temperature to produce the diazonium compound. The activated diazonium solution was then scanned using cyclic voltammetry $+0.4$ to -0.6 V (scan rate: 100 mV/s) followed by a wash with deionised water. The resulting 4-carboxyphenyl film is activated on the electrode surface with carbodiimide hydrochloride and N-hydroxysuccinimide for 60 mins to form an ester that allowed for conjugation to the amine-modified ssDNA probe.[96] The time required for the sensor to produce the result is 3.5 hrs which needs to be optimised, but it paves the way for bioanalytical sensors to be used for early detection of cancer and the monitoring the response to cancer treatment. Last, as shown within Figure 4D, Roberto de Oliveira and co-workers have fabricated a 6 individual working screen-printed arrays (SPAs) for the biosensing of serum procalcitonin (PCT).[97] PCT is a 116-amino acid polypeptide that is U.S. Food and Drug Administration approved biomarker for the assessment of the progression of infection to sepsis. It is used in aiding decisions for antibiotic therapy for patients and also for the potential de-escalation of antibiotics for septic patients when tracked over time. Concentrations of PCT have been stratified to aid interpretation where current NHS guidelines consider the normal range in adult populations to be < 0.05 ng mL^{-1}, with < 0.50 ng mL^{-1} considered to represent a low risk of sepsis and concentrations > 2.0 ng mL^{-1} reflect a high risk of sepsis. The SPAs are first modified with diazonium modification using sequential droplets. Next 4-aminobenzoic acid sodium nitrite is applied to the surface of the working electrode surface for 10 min, followed by the application of L-ascorbic acid for a further 10 min. The work electrode are cleaned where the diazonium layer was then activated using diazonium layer was then activated using N-(3-dimethylaminopropyl)-N′-ethylcarbo-diimide hydrochloride/N-(3-dimethylaminopropyl)-N′-ethylcar-bodiimide hydrochloride coupling. Procalcitonin specific anti-bodies are then attached to the surface of the working electrode surface through the application of PCT–Ab for 3 h at 4 °C. Last, the excess available surface of the working electrodes are blocked through the application of BSA for 30 min. After

being washed, the sensor is ready to use. The use of screen-printed electrodes allow the authors to design and develop a multi-sensing which allows for their mass-production, where a linear range of 1 and 10 ng mL^{-1} is feasible for sensing PCT. The use of screen-printing and the facile modification strategy provides a low cost, yet scalable approach where the material cost of the sensing platform is £1.14. The sensor was internally validated with human serum results (3 sample measurements, 3 control) for raised levels of PCT (> 2 ng mL^{-1}). No interference effects were seen from CRP and IL-6. This platform has the potential to offer clinicians imperative information to rapidly begin treatment for "query sepsis" patients while awaiting results from more lengthy remote laboratory testing methods.[97]

4.2. Screen-Printed Microelectrodes

Why would one want to change the screen-printed macro-electrode to a screen-printed microelectrode? The working area of the electrode affects the mass transport of the electroactive species to and from the electrode surface and the bulk solution, which results in low interfacial capacitive-charging currents, reduced iR drop, and steady-state diffusion currents which allows microelectrodes to be used within confined volumes.[98–100] Microelectrodes achieve an improved mass transport which exhibits a higher current density and in turn results in improved signal-to-noise ratios, since the noise levels depend on the active area of the electrode. Furthermore, microelectrodes can be used for anodic stripping voltammetry without the need for convection during the deposition step, and there is a possibility to work in low ionic strength media (absence of excess supporting electrolytes). Screen-printing provides the opportunity to modulate the dimensions of microelectrodes systematically, which affects such complex diffusion. Efforts have been directed to the design and fabrication of screen-printed microelectrodes for example, Kadara and co-workers reported micro-sized graphite screen-printed electrodes, typically with radii of 60 to 100 microns which are defined by an inert dielectric and was shown to be useful for the cathodic stripping of lead (II) ions.[101] Others have reported screen-printed diamond electrodes with various insulating polyester resin binder/boron-doped diamond powder (0.25–1 μm) and measured ascorbic acid and 8-hydroxy-2′-deoxyguanosine.[102] The boron-doped diamond powder is prepared by microwave plasma-assisted chemical vapor deposition of boron-doped diamond on to the surface of diamond power which is then mixed into graphite inks and are screen-printed.[102] The downsides of the use of microelectrodes is that a small current output is observed which can be problematic for trace analyte detection. This can be overcome via the use of a microelectrode array, where single microelectrodes are wired in parallel with each one acting diffusionally independent, generating a signal which is thousands of times larger. Microelectrode arrays, due to the large number of microelectrodes making up the array, allow for high sensitivities and low detection limits. Future work using screen-printed microelectrode should be used to the

ChemElectroChem

Review
doi.org/10.1002/celc.202400370

Chemistry Europe
European Chemical
Societies Publishing

sensing of analytes within the absence of supporting electrolytes and should explore kinetic and mechanistic information, for example it has been shown that in the absence of supporting electrolyte, that the comproportionation of anthraquinone and anthraquinone dianion proceeds at a diffusionally controlled rate in acetonitrile, a result which could not be determined from "diffusion-only" voltammetry.[103]

4.3. Screen-Printed Microelectrode Arrays

One aspect that is overlooked by those who design and fabricate their screen-printing microarrays, is the separation between the microelectrodes comprising the array,[104] which defeats their use. Wang and co-workers report the use of mercury coated ultramicroelectrode arrays for on-site stripping measurements of trace metals.[105] The approach involves the use of screen-printing onto a substrate which is then covered with a coating of a dielectric layer and exposed to laser photoablation to "drill" the desired array pattern through the dielectric film. This results in working electrodes with a diameter of 15 micrometres, separated by 160 micrometres. This is a common theme where Seddon et al[106] has reported on 15 µm diameter microelectrodes which are separated by 100 µm where the number of discs comprising the array was 3667. They showed proof-of-concept in the potentiometric sensing of cadmium (II) and lead (II) within a water sample. Others have reported the extension by those using ultrafast pulsed laser ablation where they varied the diameter of the hole from 20 to 60 µm and the array spacing ranging from 30 to 560 µm, and showed that they can produced a glucose biosensor over the range of 2.5 to 20 mM.[107] While others used the same approach to measure cadmium (II) ions using square-wave anodic stripping voltammetry (SWASV) with a detection limit of 1.3 µg L^{-1} and applied their system to detection within a river sample.[108] Other work has used sonochemical fabrication, where the graphite surface is covered by electropolymerisation, after which the researcher ablates discreet microelectrode pores via ultrasonic cavitation.[109,110] Tan et al have reported upon the fabrication of screen-printed microelectrode arrays comprised of six working electrodes (50 µm radii) which are separated from their nearest neighbour by an average distance of 2272 µm, arranged in a circular configuration around a common counter and reference electrode.[111] The electroanalytical approach was evaluated using acetaminophen, dopamine and nitrite giving LoD of 4.29, 3.24 and 5.24 µM respectively. Furthermore, using gold-based screen-printed microelectrode arrays the electroanalytical sensing of chromium (VI) can give rise to a LoD of 8.28 µM where proof-of-concept is shown through the determination of chromium (VI) within an environmental (canal water) sample.[111] In summary, these disposable and economical microelectrode arrays hold promise for in-the-field sensing applications where one can change the working electrode composition using metallic based screen-printing inks allowing the tailoring of the electrode surface enabling electrocatalytic microelectrode arrays to be readily derived.

4.4. Screen-Printed Electrode Microbands

Microband electrodes offer the enhanced sensitivity but with higher total current outputs due to the macroscopic length where the microscale width gives rise to convergent mass transport.[112] In electroanalysis, the use of microbands results in shorter response times, increased sensitivity, and lower detection limits. Through the use of screen-printing, inexpensive microbands and microband arrays can be readily fabricated; Table 3 summaries the current approaches.

As shown within Figure 7A–D, graphite microband electrodes are shown which are 10 mm in length and 100 µm in width.[116] The microscopic feature can be reduced down to 50 micrometre width with a 20 mm length[74] with the use of a high performance screen. Other approaches have used the strategy of cross-cutting to produce microbands.[75,113–115,117–127,129–131] Microband arrays have been explored within the sensing of phenolic compounds, where they compared the use of laccase-modified electrodes via direct and mediated electron transfer (see Figure 7E).[132] Laccases can undergo both direct and mediated heterogeneous electron transfer between the electrode surface and the active site of the enzyme where immobilized onto the electrode surface, laccases catalyse four-electron oxygen reduction to water via direct electron transfer, appearing as an increase of the cathodic current of oxygen reduction in the presence of the enzyme (Figure 7Ei). The authors compared the mediated electron transfer using glassy carbon (Figure 7Eii)., screen printed graphite disk electrode (Figure 7Eiii and graphite microband arrays (Figure 7Eiv) where the microband arrays gave rise to the biggest current density. This allowed the authors to measure phenol within tap and waste waters reporting a LoD of 0.009 µM and a linear range from 0.2 to 110 µM.[132] Other work has reported the use of graphite ink has been screen-printed onto a polyethylene terephthalate plastic substrate onto which five layers of insulation ink is added, this is repeated to expose the edge revealing five microbands, see Figure 6F, producing a microband array.[128] Through cyclic voltammetry measurements, the microband array length is 0.04–0.15 cm with the width corresponding to 6.3 micrometers with separation between each microband being 60 micrometers. As shown within Figure 7G, the cyclic voltammetric profiles are shown for $K_4Fe(CN)_6$ and $Ru(NH_3)_6Cl_2$ where steady-state-type current responses typical for microdimensional electrodes with enhanced mass transport of the redox material to/from the electrode due to convergent diffusion.[128]

The downside of cutting microbands is a fundamental problem which arises where cutting pulls the dielectric away from the graphite microband, which could clearly contribute to the observed (variable) electrochemical response.[116] Another useful approach is the use of screen-printed back-to-back electroanalytical sensors,[133–135] where these are screen-printed printed back-to-back with a common electrical connection to the two working electrodes and the counter and reference electrodes for each connected in the same manner as a "traditional" screen-printed electrode system. This novel approach utilises the usually redundant back of the screen-printed

ChemElectroChem

Review
doi.org/10.1002/celc.202400370

**Chemistry
Europe**
European Chemical
Societies Publishing

Table 3. A selection of the applications of microband and microband arrays screen-printed electrodes.

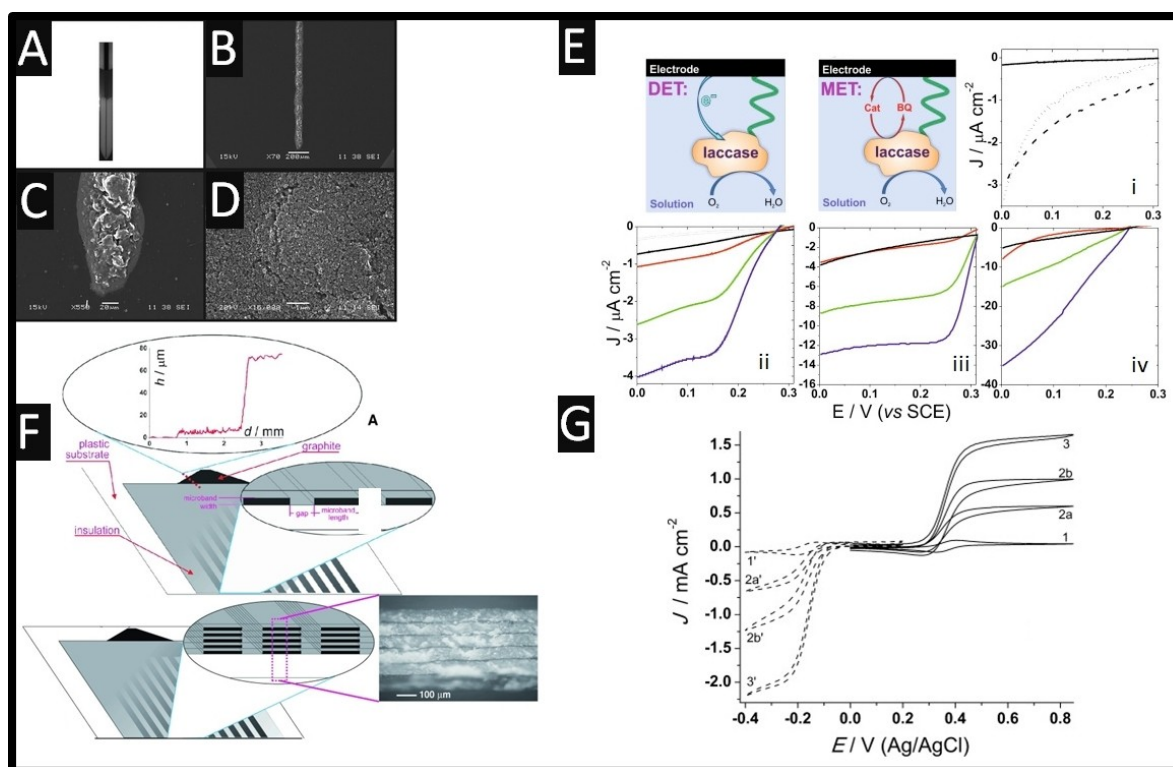| Electrode material	Description	Dimensions	Modification	Analyte/target	Dynamic range	Limit of Detection	Reference
Graphite	Single	20 μm×2 mm	None	Lead (II) ions	50 μg/L–1.70 mg/L	2.3 ng/mL	[113]
Gold	Single	6.5 mm×12 μm	None	Ascorbic acid; paracetamol	–	–	[114]
Graphite	Single	Tubular microband electrode; width 17.3 μm	Cobalt phthalocyanine	H_2O_2	1–7 mM	70 μM	[115]
Graphite	Single	100 μm×10 mm	None	NADH; nitrite	**1–100** μM; 10–700 μM	0.48;0.05 μM	[116]
Graphite	Single	50 μm×20 mm	None	NADH	1–10 μM	0.24 μM μM	[74]
Gold	Single	50 μm×20 mm	None	Chromium (VI)	10–100 μM	2.65 μM	[74]
Gold	Single	17 μm×1.5 mm	None	Arsenic (III)	0–20 μg/L	0.8 μg/L	[75]
Graphite	Single	20 μm×0.18 mm	None	Nitrite	5 μM–3 mM	0.38 μM	[117]
Graphite	Single	20 μm×0.18 mm	None	Nitrite, iodide	NR	0.38 μM; NR	[118]
Graphite	Single	20 μm×0.18 mm	Pt NPs	CO	47–1000 ppm	28.6 ppm	[119]
Graphite	Single	20 μm×0.18 mm	Pt NPs/Nafion®	formaldehyde	0.3–5.1 ppm	80 ppb	[120]
Graphite	Single	17.6 μm×3 mm	CoPC/Lactate Oxidase	Lactate via H_2O_2	1–6 mM	289 μM	[121]
Graphite	Single	20 μm×3 mm	CoPC/Glucose Oxidase	Glucose	0.45–9 mM	NR	[122]
Graphite	Single	20 μm×3 mm	CoPC/Glucose Oxidase	Glucose	5–10 mM	NR	[123]
Graphite	Single	20 μm×3 mm	CoPC/Glucose Oxidase	Glucose	0.5–7 mM	0.27 mM	[122]
Graphite	Single	20 μm×0.18 mm	PtRu NPs	Glycerol	0.92–92 mg/L	0.51 mg/L	[124]
Graphite	Single	20 μm×0.18 mm	Pt NPs/Nafion®	NO; Nitrite	38.50–666.66 ppm; 0.2–1000 μM	NR; 3.7 nM	[125]
Graphite	Single	20 μm×0.18 mm	None	Nitrite	1–600 μM	0.0067 μM	[126]
Graphite	Single	20 μm×1.4 mm	Bismuth	Cadmium (II) ions	5–45 μg/L	1.3 μg/L	[127]
Gold	Array	6.5 mm×12 μm	None	Thiamine	–	–	[114]
Graphite	Array	6.3 μm×0.04–0.15 cm	None	Ascorbic acid; glucose	NR; 1–30 mM	NR	[128]
Graphite	Array	4.76 μm×1.42 mm	Gold nanoparticles; indirect approach measuring gold (III) ions	Amplified Human Cytomegalovirus DNA	5–500 pM	5 pM	[129]

Key: CoPC: cobalt phthalocyanine; NR: not reported; Pt NPs: platinum nanoparticles.

electrode, converting this "dead-space" into an enhanced screen-printed electrode configuration which results in improvements in the electroanalytical performance. Furthermore, rather than screen-printing onto the back of a screen-printed electrode, one can take two electrodes and simply place them back-to-back. In this design, the electrode area is consequently doubled with improvements in the electroanalytical performance observed with the analytical sensitivity (gradient of a plot of peak height/analytical signal against concentration) doubling and the corresponding LoD being reduced.[133–135]

5. Bulk Modified Screen-Printed Electrodes

When someone wishes to modify their electrode with a desired material, for example carbon nanotubes, one approach is the use of drop-casting. In this way, a drop of liquid containing a suspension of the carbon nanotubes is deposited onto the electrode surface, which the liquid is left to evaporate leaving the carbon nanotubes being deposited. If done incorrectly, due to Marangoni effects, one can observe a coffee ring affect where the distribution across of the surface is altered which has a negative influence in (electro)analytical chemistry resulting in inhomogeneity to target analytes and results in poor stability.[136–138] The approach to circumvent the coffee-ring effect, is to modify the screen-printed ink with the desired material which reduces the resistance between the desired material and the electrode surface and improves electron transfer properties. It provides a simple but effective approach, allowing one to create mass-produced electrochemical platforms. As shown within Table 4, one can observe the range of modifications and their use. For example, cobalt phthalocyanine bulk modified screen-printed electrode have been extensively explored towards key analytes including citric acid determined in lime juice and fruit,[139] thiocholine,[140] glutathione,[141] glucose,[107] lactate,[142] Vitamin B1,[143] organophosphates,[144]

ChemElectroChem

Review
doi.org/10.1002/celc.202400370

Chemistry Europe
European Chemical
Societies Publishing

Figure 7. A–D: Optical and scanning electron microscopy images of the 50 μm graphite microband. Figure reproduced from reference.[74] Copyright 2013 The Royal Society of Chemistry. E: Bioelectrocatalysis on laccase-modified carbon electrodes. A and B represent the schemes of direct electron transfer (DET) and mediated electron transfer (MET), respectively, Cat and BQ are catechol and benzoquinone, respectively. i: DET on laccase-modified electrodes. Background-subtracted linear sweep voltammograms obtained at laccase-modified glassy carbon, screen printed graphite disk electrode and graphite microband arrays (solid, dotted and dashed curves, respectively) in air-saturated buffer. ii, iii and iv: MET on laccase-modified glassy carbon, screen printed graphite disk electrode and graphite microband arrays respectively. Linear sweep voltammograms obtained after addition of 0, 10, 50 and 100 μM (black, red, green and blue curves, respectively) of catechol; 0.1 M acetate buffer, the scan rate is $1\ mV\,s^{-1}$. Figure reproduced from reference.[132] Copyright 2016 Elsevier. F: Cyclic voltammograms of the using screen-printed graphite microband electrode arrays within 1 mM solution of $K_4Fe(CN)_6$ (curves 1, 2a, 2b, and 3) and a 1 mM solution of $Ru(NH_3)_6Cl_2$ (dashed curves 1', 2a', 2b', and 3') in 0.1 M HCl, scan rate $50\ mV\,s^{-1}$ which shows the macroelectrode (curves 1 and 1', same as a), the multilayer array (curves 2a and 2a', same as a), the single-layer microband array (0.4 mm length, curves 2b and 2b'), and the single microelectrode (diameter: 7 μm, curves 3 and 3'). Figure reproduced from reference.[128] Copyright 2014 Chemistry Europe Journal. G: An overview of the screen-printed graphite microband electrode arrays. A single-layer array with profilometer data is shown and a multilayer array of five electrode layers. The optical microscopy image shows the graphite layers as five dark interfacial layers.

esterified fatty acids,[145] polyunsaturated fatty acids,[146] and cysteine,[147] to name just a few. These approaches are limited since they are using commercially available cobalt phthalocyanine modified ink which can only be bought at one loading (% 5 (m/m)).[144] To overcome this limitation, others have modified graphite ink with various amount of the bulk modification, for example, where bismuth oxide is added over the range, typically from 1–15% (M_P/M_I), where M_P is the mass of particulate and M_I is the mass of ink formulation used in the printing process.[148–150] Such bismuth oxide bulk modified screen-printed electrodes have been explored toward the sensing of lead (II) and cadmium (II) in water and soil samples[150] and zinc (II) within seawater where linear range and LoD is in accordance with monitoring levels set by the World Health Organisation and USA Environmental Protection Agency.[149] Other approaches have used related electrochemical processes, for example bespoke bulk modified electrodes incorporating the materials of 2D-hBN and MoS_2 have been evaluated towards the oxygen reduction reaction[151,152] and the hydrogen evolution reactions using MoSe2, WS_2, and

Fe_3P.[153–155] Both reactions are essential processes in electrochemistry for energy conversion within fuel cells. Other interesting work has used the benefit of graphene oxide which exhibits electrochemical sensing properties dependant on the high C/O content. Researchers studied the effect of different % of GO from 2.5 up to 10% where the 10% GO bulk modified screen-printed electrodes exhibited the high sensitivity and gave a linear range towards dopamine and uric acid with a LoD of 0.78 and 2.3 μM respectively.[156] The electrodes were explored towards the intra-repeatability where using 50 μM towards the sensing of dopamine which gave rise to % RSDs of 2.2, 3.4, 5.1 and 5.8 for 2.5, 5, 7.5 and 10% GO bulk modified screen-printed electrodes respectively. Other work has reported the use of zeolite nanocrystals for the simultaneous detection of methocarbamol and paracetamol which gave a linear range of 0.4 μM–0.1 mM, with LoDs of 86 nM and 80 nM respectively.[157] Methocarbamol, 2-Hydroxy-3-(2-methoxyphenoxy)-propyl carbamate, is a muscle relaxant drug used to treat muscle pain and discomfort caused by muscle spasm or cramps where they also measured paracetamol, a common painkiller,

ChemElectroChem

Review
doi.org/10.1002/celc.202400370

Chemistry Europe
European Chemical
Societies Publishing

Table 4. A selection of the bulk modified screen-printed electrodes reported using graphite screen-printed electrodes.

Bulk modification	Analyte/target	Dynamic range	Limit of Detection	Reference
Cobalt phthalocyanine	Thiocholine	0.5–48 μM	–	[140]
Cobalt phthalocyanine	lactate	18.3 μM–1.5 mM	18.3 μM	[142]
Cobalt phthalocyanine	Citric acid	2 mM–2 M	0.2 M	[139]
2D-hBN	ORR	–	–	[151]
MoSe$_2$	HER	–	–	[153]
MnO$_2$	Ascorbic acid	50–250 mg/L	0.2 mg/L	[158]
Fe$_3$P	HER	–	–	[155]
lactate oxidase and horseradish peroxidase	Lactate	10–180 μM	–	[159]
MoS$_2$	ORR	–	–	[152]
GO	Dopamine; uric acid	5–50 μM; 20–200 μM	0.78;2.3 μM	[156]
MIP	Glucose	1.37–330 μM	1.37 μM	[160]
Calixarene	Lead (II), copper (II) and mercury (II)	100–2400 μg/L	38, 40, 48 μg/L	[161]
WS$_2$	HER	–	–	[154]
GO	Supercapacitor	–	–	[162]
Resazurin	Urinary tract infections	–	15.6 μM	[163]
Prussian blue	H$_2$O$_2$	0.4–100 μM	0.4 μM	[164]
Prussian blue-Ammine	Cysteine	100–600 μM	67.4 μM	[165]
Prussian blue-Ammine	Cysteine	300–800 μM	149.3 μM	[165]
Cyclodextrin functionalized reduced graphene oxide	Cysteine	0.5–170 μM	0.12 μM	[166]
N′-phenyl-p phenyldiamine/multiwalled carbon nanotubes	Dopamine	1–110 μM	0.01 μM	[167]
Bismuth oxide	Zinc (II) ions	75–600 μg/L	33 μg/L	[149]
MnO$_2$ and glucose oxidase	Glucose	11–13900 μM	1 μM	[168]
Bismuth oxide	Lead (II), cadmium (II)	20–300 μg/L	8 μg/L; 16 μg/L	[150]
Bismuth oxide	Lead (II), cadmium (II) and zinc(II) ions	10–150 μg/L	5, 10 and 30 μg/L	[148]
Anthraquinone-2-COOH-cysteamine	Oxygen	0.2–6.1 mg/L	0.13 mg/L	[169]
Prussian blue and glucose oxidase	Glucose	1–4 mM	0.2 mM	[170]
Antimony oxide	Cadmium (II)	25–100 μg/L	20 μg/L	[171]
Zeolite nanocrystals	Methocarbamol and Paracetamol simultaneously	0.4 μM–0.1 mM	86 nM; 80 nM	[157]

Key: GO: graphene oxide; hBN: Hexagonal *boron nitride;* HER: hydrogen evolution reaction; MIP: molecular imprinted polymer; ORR: oxygen reduction reaction.

which they showed that the voltammetric peaks are well-resolved and furthermore, they showed their sensing performs in the presence of ascorbic acid and uric acid.[157]

Bulk modified screen-printed electrodes have opened up avenues for sensitive and selective electrochemical applications and their use within electroanalysis where researchers should continue to explore their use for improved their performance for specific applications. Future work should continue to expand the use of bulk modified screen-printed electrodes incorporating novel micro/nano materials and associated metal oxides towards the sensing of interesting but yet diverse analytes.

6. Activation of Screen-Printed Electrodes

While screen-printed electrodes are design to be used a disposable, single-shot device that one can be used without pretreatment, others have utilised pretreatment processes in order to activate their electrode. This can help improve electron transfer, hydrophilicity, conductivity, roughness, charge density, activity, loading capacity and the removal surface contaminants. This can be done via physical and/or chemical methods and can also help with the modification of biological recognition elements such as enzymes, proteins, antibodies and nucleic acids. The predominant approach is electrochemical pretreatment, but others have used oxygen plasma, heat treatment, mechanical and ultrasonic polishing to name just a few.[172–175]

For example, Wang and co-workers[176] have explored an electrochemical pretreatment using screen-printed graphite electrodes which involved holding the potential for 3 min at +2.0 V, which improved the electrochemical sensing of acetaminophen, cysteine, tyrosine, uric acid and catechol, as shown in Figure 8A. One can observe that there was a dramatic improvement in the electron transfer kinetics and a significant background current enhancement after activation. Through the use of X-ray photoelectron spectroscopy (XPS) the authors reports that the oxygen-to-carbon ratio increased from 0.32 to 0.50 following electrochemical activation. Through the use of voltammetric, microscopic and spectroscopic approaches, they concluded that the electrochemical pretreatment increased surface functionalities and roughness or removed surface contaminants. On further inspection of the electrochemical pretreatments, there are many that can be mentioned, for example, the application of +1.2 V for 20 second in 0.5 NaOH which showed a beneficial response towards dopamine,[177] others have used −1.2 V for 20 s within 0.1 NaOH which was shown to be beneficial to the measurement of dopamine,[178] similarly the potential was cycled from 0.0 to +2.0 V for 10 cycles within 0.1 NaOH which was shown to be beneficial to the sensing of gallic acid,[179] but both accounts report that both underwent adsorption controlled process,[177–179] hinting the presence of increased oxygen content, but no evidence is provided on the C/O groups and their identification. Figure 8B shows an electrochemically activated screen-printed graphite

electrode that was treated using 0.5 M H_2SO_4 and 0.01 M H_2O_2. This involved 10 consecutive voltammetric cycles between +2 and −0.3 V at 100 mV s^{-1}, followed by 25 consecutive voltammetric cycles between +1 and −0.7 V at 10 mV s^{-1}.[180] From observation of the Figure 8B, one can see the dramatic effects of the electrochemical pretreatment, giving rise to faster electron transfer properties facilitated by the formed oxygenate species. Using XPS, the authors show that the at.% carbon is 94.17% where the at.% oxygen is 5.65% before electrochemical activation which changes to at.% carbon is 77.89% where the at.% oxygen is 21.06%.[180] This is then presented into the different C/O groups which reports a high C—O to C=O ration as well presence of OH groups in carboxyl functionalisation.[180] In comparison for the electroanalysis of hydrogen peroxide, where using an unmodified screen-printed graphite electrode gave rise to a sensitivity of 1.7 nA μM^{-1} cm^{-2}, after treatment this improved to 881 nA μM^{-1} cm^{-2}, which shows the power of electrochemical activation. Another approach worthy of note, is the work by Chen and co-workers[181] where an electrochemically pretreated screen-printed graphite electrode, evidenced via XPS, which gave rise to hydroxyl (C—OH) functionalities and mixtures of carboxylic and carbonyl functional groups (—C=O-(OH)), which supports the hydrogen evolution reaction. See Figure 8C, which shows the details on how they electrochemically pretreated their screen-printed carbon electrode, where negligible signals are transformed into distinctive hydrogen evolution reaction curves. The hydrogen evolution reaction
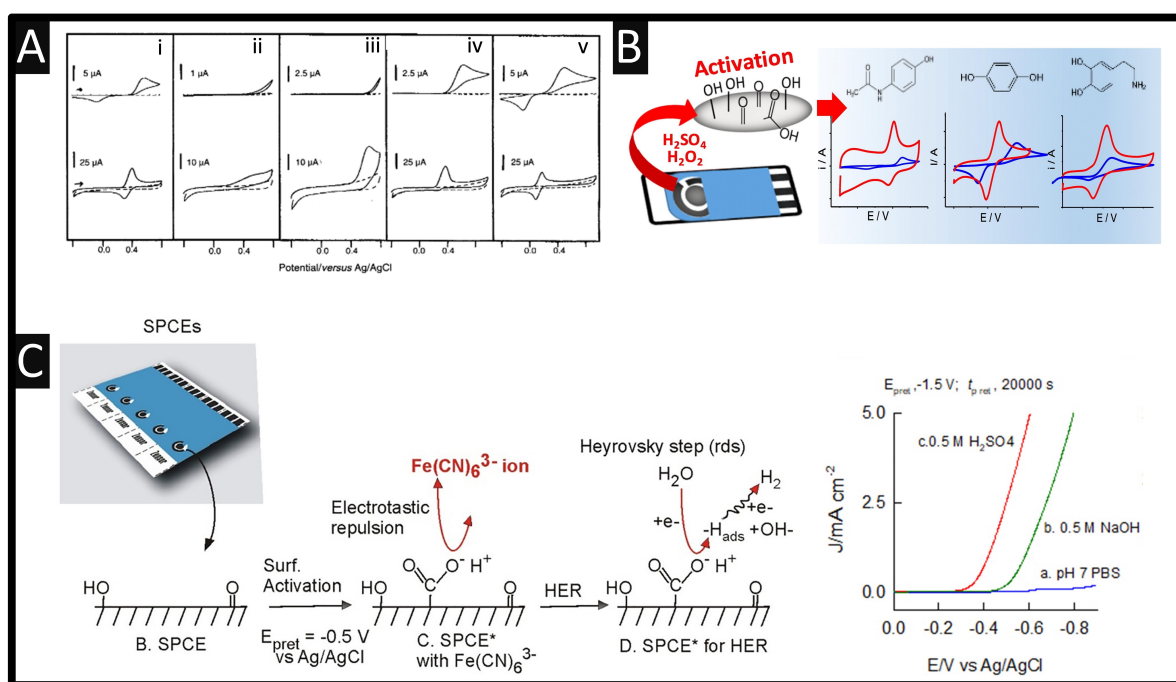
Figure 8. A: Cyclic voltammograms for 1 mM i, acetaminophen; ii, cysteine; iii, tyrosine; iv, uric acid; and v, catechol at the untreated (top) and electrochemically pretreated (bottom) screen-printed graphite electrodes. Pretreatment (bottom), 3 min at +2.0 V; scan rate, 50 mV s^{-1} within supporting electrolyte, 0.05 M phosphate buffer. Dashed lines correspond to the response of the blank buffer solution. Figure reproduced from reference.[176] Copyright 1996 The Royal Society of Chemistry. B: Electrochemical activating using screen-printed graphite electrodes. Figure reproduced from reference.[180] Copyright 2019 Elsevier. C: An overview of surface pre-treatment of screen-printed graphite electrodes and its assistance for the effective hydrogen evolution reaction in 0.5 M H_2SO_4 following Heyrovsky type of reaction mechanism. Also shown is linear sweep voltammetric response of pre-treated screen-printed graphite electrodes at −1.5 V vs Ag/AgCl for 20,000s in pH7 PBS (a), 0.5 M NaOH (b) and 0.5 M H2SO4 (c). Figure reproduced from reference.[181] Copyright 2019 Elsevier.

proceeds with two rate-determining step (rds): (i) hydrated proton associates with electron and chemically attach on the electrode surface (Volmer step; $H_2O + e^- \rightarrow H_{ads} + OH^-$; *Tafel plot* $= 120$ mV dec^{-1}); ii(a) the adsorbed proton, (H_{ads}) combined with hydrated proton and electron from the electrode (Heyrovsky step; $H_2O + e^- + H_{ads} \rightarrow H_2 + OH^-$; *Tafel plot* $= 40$ mV dec^{-1}) or ii(b) direct combination of H_{ads} (Tafel step: $H_{ads} + H_{ads} \rightarrow H_2$: *Tafel plot* $= 30$ mV dec^{-1}). The authors measured the Tafel plot where they observed 54.7 mV dec^{-1} which is close to the value 40 mV dec^{-1}, it is proposed that Heyrovsky step is the rds of the overall reaction.[181] Many authors presume that the electrochemical activation provides C/O functionalities but there are many who do not provide concluding evidence; future work should be backed-up with XPS and associated characterisation to confirm the amount and type of the C/O functionalities.

Other approaches use simple mechanical activation/polishing techniques to activate screen-printed graphite electrodes which can beneficially change the oxygen content upon the electrode surface. The introduction of new carbon–oxygen groups, validated with XPS improves electron transfer rate kinetics for inner-sphere redox systems only.[182] Others have compared platinum and gold screen-printed electrodes using polar solvents and hydrogen peroxide where hydrogen peroxide and multiple cyclic voltammograms gave rise to the most efficient cleaning method.[183]

In summary, electrochemical pretreatment provides interesting results where others should explore this to further extend their beneficial use and applications. Such approaches are empirical in nature and when electrochemical activation is used, physicochemical characterisation of the C/O content should be performed otherwise there is little point of reporting data that cannot be easily reproduced by others.

7. Changing the Connection Length of the Screen-Printed Electrodes

The connection length of screen-printed electrodes has been consistent after Wring *et al.*[184] were the first to report in detail on the preparation of screen-printed carbon based electrodes. They produced a rectangular screen-printed electrode composed of a 3 mm circular working electrode with a 25×1 mm wide connecting strip and an electrode 100 mm in length. This working size of the electrode offers comparison with other commercially available working electrodes, such as metallic and glassy carbon electrodes. Whittingham and co-workers[16] have shown that by changing the connection length from 32 mm down to 12 mm, more accurate heterogeneous electrode kinetics can be calculated, which cannot be overcome through IR compensation. Reducing the connection length results in lower resistance. In the case of electroanalytical sensing, the authors explored the sensing of sodium nitrite, β-nicotinamide adenine dinucleotide (NADH), and lead (II) where significant improvement are observed when using the shortest connection length. This work suggests that as a benchmark, authors should report the resistance and the connection lengths of the screen-

printed electrodes. The same concept has been extended to additive manufacturing electrodes where reducing the connection length results in a reduction in the resistance which improves the electrochemical and electroanalytical performance.[185] In summary, future work should report their electrochemical resistance and also explore the concept laid out by Whittingham and co-workers[16] by changing the length of the electrode of screen-printed electrodes in order to optimise electroanalytical performance.

8. Conclusions

In this review we discuss screen-printed electrodes, including manufacturing and use with standard and alternative materials, modification of electrodes through drop-casting and bulk ink modification, microelectrodes and arrays, activation of electrodes, and how geometric changes to the electrode affect the performance. Screen-printed electrodes are ubiquitous within the field of electroanalytical chemistry, with huge amounts published papers reporting their use. Even so, there are still significant parameters to explore to maximize their performance and expand their commercial use into other areas. One relevant aspect is the use of life cycle analysis where it can be used for the quantification of the sustainability of the large-scale production and the materials used *e.g.*, inks, solvents, substrates, micro/nanomaterials *etc.* involved in screen-printing of electrodes; further work should be explored in expanding this research aspect. One area that needs considerable attention is the disposal and waste aspects of their use. As these electrodes are commonly produced on plastic substrates and are used as single-use items, wide uptake in their use could result in significant issues with plastic pollution. As such greener manufacturing techniques and appropriate recycling methods should be developed.

Conflict of Interests

The authors declare no conflict of interest.

Data Availability Statement

Research data are not shared.

[1] A. J. Bandodkar, V. W. S. Hung, W. Jia, G. Valdés-Ramírez, J. R. Windmiller, A. G. Martinez, J. Ramírez, G. Chan, K. Kerman, J. Wang, *Analyst* **2013**, *138*, 123–128.

[2] Y.-L. Yang, M.-C. Chuang, S.-L. Lou, J. Wang, *Analyst* **2010**, *135*, 1230–1234.

[3] K. Malzahn, J. R. Windmiller, G. Valdés-Ramírez, M. J. Schöning, J. Wang, *Analyst* **2011**, *136*, 2912–2917.

[4] J. P. Metters, S. M. Houssein, D. K. Kampouris, C. E. Banks, *Anal. Methods* **2013**, *5*, 103–110.

ChemElectroChem

Review

doi.org/10.1002/celc.202400370

Chemistry Europe
European Chemical
Societies Publishing

[5] A. J. Bandodkar, W. Jia, J. Wang, *Electroanalysis* **2015**, *27*, 562–572.

[6] F. Chen, J. Wang, L. Chen, H. Lin, D. Han, Y. Bao, W. Wang, L. Niu, *Anal. Chem.* **2024**, *96*, 3914–3924.

[7] R. García-González, M. T. Fernández-Abedul, A. Pernía, A. Costa-García, *Electrochim. Acta* **2008**, *53*, 3242–3249.

[8] S. Singh, J. Wang, S. Cinti, *ECS Sens. Plus* **2022**, *1*, 023401.

[9] A. García-Miranda Ferrari, S. J. Rowley-Neale, C. E. Banks, *Talanta Open* **2021**, *3*, 100032.

[10] J. P. Metters, R. O. Kadara, C. E. Banks, *Analyst* **2011**, *136*, 1067–1076.

[11] R. O. Kadara, N. Jenkinson, C. E. Banks, *Sens. Actuators B* **2009**, *138*, 556–562.

[12] A. García-Miranda Ferrari, P. Carrington, S. J. Rowley-Neale, C. E. Banks, *Environ. Sci. Water Res. Technol.* **2020**, *6*, 2676–2690.

[13] A. G.-M. Ferrari, R. D. Crapnell, C. E. Banks, *Biosensors* **2021**, *11*, 291.

[14] M. Li, Y.-T. Li, D.-W. Li, Y.-T. Long, *Anal. Chim. Acta* **2012**, *734*, 31–44.

[15] K. K. Mistry, K. Layek, A. Mahapatra, C. RoyChaudhuri, H. Saha, *Analyst* **2014**, *139*, 2289–2311.

[16] M. J. Whittingham, N. J. Hurst, R. D. Crapnell, A. Garcia-Miranda Ferrari, E. Blanco, T. J. Davies, C. E. Banks, *Anal. Chem.* **2021**, *93*, 16481–16488.

[17] H. M. A. Amin, Y. Uchida, E. Kätelhön, R. G. Compton, *J. Electroanal. Chem.* **2021**, *880*, 114891.

[18] Z. Żołek-Tryznowska, in *6 - Rheology of Printing Inks, Vol.* (Eds: J. Izdebska, S. Thomas), William Andrew Publishing **2016**, pp.87–99.

[19] M. Albareda-Sirvent, A. Merkoçi, S. Alegret, *Sens. Actuators B* **2000**, *69*, 153–163.

[20] N. B. Mincu, V. Lazar, D. Stan, C. M. Mihailescu, R. Iosub, A. L. Mateescu, *Diagnostics (Basel, Switzerland)* **2020**, *10*.

[21] M. Sharafeldin, A. Jones, J. F. Rusling, *Micromachines* **2018**, *9*, 394.

[22] A. Hayat, J. L. Marty, *Sensors* **2014**, *14*, 10432–10453.

[23] M. Li, D.-W. Li, G. Xiu, Y.-T. Long, *Curr. Opin. Electrochem.* **2017**, *3*, 137–143.

[24] A. Vasilescu, G. Nunes, A. Hayat, U. Latif, J.-L. Marty, *Sensors* **2016**, *16*, 1863.

[25] M. R. Somalu, A. Muchtar, W. R. W. Daud, N. P. Brandon, *Renewable Sustainable Energy Rev.* **2017**, *75*, 426–439.

[26] J. P. Mensing, T. Lomas, A. Tuantranont, *Sustainable Mater. Technol.* **2020**, *25*, e00190.

[27] A. Economou, *Sensors* **2018**, *18*, 1032.

[28] L. Pereira de Oliveira, D. P. Rocha, W. Reis de Araujo, R. A. Abarza Muñoz, T. R. Longo Cesar Paixão, M. Oliveira Salles, *Anal. Methods* **2018**, *10*, 5135–5163.

[29] C. S. Ong, Q. H. Ng, S. C. Low, *Monatsh. Chem. – Chem. Monthly* **2021**, *152*, 705–723.

[30] M. A. Alonso-Lomillo, O. Domínguez-Renedo, M. J. Arcos-Martínez, *Talanta* **2010**, *82*, 1629–1636.

[31] C. E. Banks, C. W. Foster, R. O. Kadara, *Screen-Printing Electrochemical Architectures*, Springer International Publishing **2015**.

[32] R. M. Silva, A. D. da Silva, J. R. Camargo, B. S. de Castro, L. M. Meireles, P. S. Silva, B. C. Janegitz, T. A. Silva, *Biosensors* **2023**, *13*, 453.

[33] F. Arduini, L. Micheli, D. Moscone, G. Palleschi, S. Piermarini, F. Ricci, G. Volpe, *TrAC Trends Anal. Chem.* **2016**, *79*, 114–126.

[34] Z. Taleat, A. Khoshroo, M. Mazloum-Ardakani, *Microchim. Acta* **2014**, *181*, 865–891.

[35] M. Tudorache, C. Bala, *Anal. Bioanal. Chem.* **2007**, *388*, 565–578.

[36] S. Cinti, F. Arduini, *Biosens. Bioelectron.* **2017**, *89*, 107–122.

[37] J. Barton, M. B. G. García, D. H. Santos, P. Fanjul-Bolado, A. Ribotti, M. McCaul, D. Diamond, P. Magni, *Microchim. Acta* **2016**, *183*, 503–517.

[38] H. M. Mohamed, *TrAC Trends Anal. Chem.* **2016**, *82*, 1–11.

[39] J. R. Windmiller, J. Wang, *Electroanalysis* **2013**, *25*, 29–46.

[40] J. Wang, M. Musameh, *Analyst* **2004**, *129*, 1–2.

[41] C. Boero, S. Carrara, G. Del Vecchio, L. Calzà, G. De Micheli, *Sens. Actuators B* **2011**, *157*, 216–224.

[42] J. P. Metters, M. Gomez-Mingot, J. Iniesta, R. O. Kadara, C. E. Banks, *Sens. Actuators B* **2013**, *177*, 1043–1052.

[43] C. Karuwan, A. Wisitsoraat, P. Chaisuwan, D. Nacapricha, A. Tuantranont, *Anal. Methods* **2017**, *9*, 3689–3695.

[44] E. P. Randviir, D. A. C. Brownson, J. P. Metters, R. O. Kadara, C. E. Banks, *Phys. Chem. Chem. Phys.* **2014**, *16*, 4598–4611.

[45] J. P. Smith, C. W. Foster, J. P. Metters, O. B. Sutcliffe, C. E. Banks, *Electroanalysis* **2014**, *26*, 2429–2433.

[46] J. Ping, J. Wu, Y. Wang, Y. Ying, *Biosens. Bioelectron.* **2012**, *34*, 70–76.

[47] C. Zanoni, R. Rovida, L. R. Magnaghi, R. Biesuz, G. Alberti, *Chemosensors* **2022**, *10*, 517.

[48] M. Antipchik, J. Reut, A. G. Ayankojo, A. Öpik, V. Syritski, *Talanta* **2022**, *250*, 123737.

[49] L. Yan, B. Luo, C. Wang, H. Dong, X. Wang, P. Hou, K. Liu, A. Li, *ChemElectroChem* **2024**, *11*, e202300538.

[50] F. W. L. Silva, L. L. Name, D. Y. Tiba, B. F. Braz, R. E. Santelli, T. C. Canevari, F. H. Cincotto, *Talanta* **2024**, *266*, 125075.

[51] A. V. Kolliopoulos, J. P. Metters, C. E. Banks, *Anal. Methods* **2013**, *5*, 851–856.

[52] A. V. Kolliopoulos, J. P. Metters, C. E. Banks, *Anal. Methods* **2013**, *5*, 3490–3496.

[53] F. D. Gonçalves, J. A. Rodrigues, R. M. Ramos, *Chemosensors* **2023**, *11*, 575.

[54] S. Thiruvottriyur Shanmugam, R. Van Echelpoel, G. Boeye, J. Eliaerts, M. Samanipour, H. Y. V. Ching, A. Florea, S. Van Doorslaer, F. Van Durme, N. Samyn, M. Parrilla, K. De Wael, *ChemElectroChem* **2021**, *8*, 4826–4834.

[55] J. Kozak, K. Tyszczuk-Rotko, *ECS Meet. Abstracts* **2021**, *MA2021–01*, 1997.

[56] G. Kaleli-Can, B. Ozlu, H. F. Özgüzar, B. Onal-Ulusoy, G. Kabay, T. Eom, B. S. Shim, M. Mutlu, *Electroanalysis* **2020**, *32*, 1696–1706.

[57] P. A. Raymundo-Pereira, N. O. Gomes, J. H. S. Carvalho, S. A. S. Machado, O. N. Oliveira Jr., B. C. Janegitz, *ChemElectroChem* **2020**, *7*, 3074–3081.

[58] Z. Liang, S. Hu, Y. Peng, C. Cheng, J. Luo, L. Yang, M. Yang, X. Yu, Y. Zhao, Z. Su, *IEEE Sens. J.* **2024**, *24*, 71–77.

[59] V. Abhikha Sherlin, M. M. Stanley, S.-F. Wang, B. Sriram, J. N. Baby, M. George, *Food Chem.* **2023**, *423*, 136268.

[60] G. Padmalaya, K. H. Vardhan, P. S. Kumar, M. A. Ali, T.-W. Chen, *Chemosphere* **2022**, *288*, 132560.

[61] P. Laolue, J. Lerdsri, *J. Food Compos. Anal.* **2023**, *124*, 105699.

[62] K. Torres-Rivero, C. Pérez-Ràfols, J. Bastos-Arrieta, A. Florido, V. Martí, N. Serrano, *Nanomaterials* **2020**, *10*, 1280.

[63] M. Zouari, R. Barderas, J. M. Pingarrón, N. Raouafi, S. Campuzano, *Sens. Actuators B* **2024**, *401*, 135017.

[64] S. Cotchim, S. Kongkaew, P. Thavarungkul, P. Kanatharana, W. Limbut, *Talanta* **2024**, *272*, 125755.

[65] İ. Okman Koçoğlu, P. E. Erden, E. Kılıç, *Anal. Biochem.* **2024**, *684*, 115387.

[66] G. Martins, H. R. Galeski, G. A. Andrade, M. G. P. Valenga, M. K. Ramos, A. J. G. Zarbin, B. C. Janegitz, M. Müller-Santos, E. M. de Souza, L. H. Marcolino-Junior, M. F. Bergamini, *Anal. Chim. Acta* **2023**, *1278*, 341726.

[67] L. M. A. Melo, L. C. Arantes, D. M. Pimentel, A. A. Macedo, R. M. Verly, E. S. Gil, W. T. P. dos Santos, *Sens. Actuators B* **2023**, *393*, 134183.

[68] S. Garg, A. Singh, A. S. Parmar, Rosy, *ACS Appl. Nano Mater.* **2023**, *6*, 14849–14860.

[69] J. L. D. Nelis, D. Migliorelli, L. Mühlebach, S. Generelli, L. Stewart, C. T. Elliott, K. Campbell, *Talanta* **2021**, *228*, 122215.

[70] R. Cancelliere, A. Di Tinno, A. M. Di Lellis, G. Contini, L. Micheli, E. Signori, *Biosens. Bioelectron.* **2022**, *213*, 114467.

[71] E. M. Materón, A. Wong, T. A. Freitas, R. C. Faria, O. N. Oliveira, *J. Pharm. Anal.* **2021**, *11*, 646–652.

[72] J. P. Metters, R. O. Kadara, C. E. Banks, *Analyst* **2012**, *137*, 896–902.

[73] J. Kozak, K. Tyszczuk-Rotko, *Measurement* **2023**, *217*, 113107.

[74] J. P. Metters, R. O. Kadara, C. E. Banks, *Analyst* **2013**, *138*, 2516–2521.

[75] R. Dudeney, J. D. Newman, F. Davis, S. J. Setford, I. E. Tothill, *Electroanalysis* **2017**, *29*, 2332–2339.

[76] M. Revenga-Parra, S. N. Robledo, E. Martínez-Periñán, M. M. González-Quirós, A. Colina, A. Heras, F. Pariente, E. Lorenzo, *Sens. Actuators B* **2020**, *312*, 127848.

[77] A. Karczmarczyk, A. J. Baeumner, K.-H. Feller, *Electrochim. Acta* **2017**, *243*, 82–89.

[78] D. C. Ferreira, M. R. BatisMtuti, B. Bachour, M. Mulato, *Bioelectrochemistry* **2021**, *137*, 107586.

[79] S. H. Kim, O. Nam, E. Jin, M. B. Gu, *Biosens. Bioelectron.* **2019**, *123*, 160–166.

[80] F. Arduini, S. Guidone, A. Amine, G. Palleschi, D. Moscone, *Sens. Actuators B* **2013**, *179*, 201–208.

[81] A. Zolfaghari Asl, A. A. Rafati, S. Khazalpour, *J. Mol. Liq.* **2023**, *369*, 120942.

[82] I. Albalawi, A. Hogan, H. Alatawi, S. Alsefri, E. Moore, *Sens. Actuators B* **2023**, *380*, 133273.

[83] H. D. Hernández, R. B. Dominguez, J. M. Gutiérrez, *Eng. Proc.* **2023**, *35*, 1.

[84] K. Choowongkomon, J. Chaisakul, S. Seetaha, T. Vasaruchapong, W. C. Hodgson, N. Rasri, K. Chaeksin, S. Boonchaleaw, N. Sookprasert, *Toxin Rev.* **2024**, *16*, 56.

[85] I. L. de Mattos, L. Gorton, T. Ruzgas, *Biosens. Bioelectron.* **2003**, *18*, 193–200.

[86] J. P. Metters, F. Tan, R. O. Kadara, C. E. Banks, *Anal. Methods* **2012**, *4*, 1272–1277.

[87] J. P. Metters, F. Tan, C. E. Banks, *J. Solid State Electrochem.* **2013**, *17*, 1553–1562.

[88] B. Thakur, E. Bernalte, J. P. Smith, C. W. Foster, P. E. Linton, S. N. Sawant, C. E. Banks, *Analyst* **2016**, *141*, 1233–1238.

[89] S. Tvorynska, J. Barek, B. Josypcuk, *Electrochim. Acta* **2023**, *445*, 142033.

[90] A. K. M. S. Inam, M. A. Costa Angeli, B. Shkodra, A. Douaki, E. Avancini, L. Magagnin, L. Petti, P. Lugli, *ACS Omega* **2021**, *6*, 33523–33532.

[91] A. K. M. S. Inam, M. A. C. Angeli, A. Douaki, B. Shkodra, P. Lugli, L. Petti, *Sensors* **2022**, *22*, 2754.

[92] F.-C. Kuo, C.-Y. Huang, Y.-T. Lin, H.-y. Tsai, *J. Pharm. Biomed. Anal.* **2023**, *235*, 115646.

[93] O. Pourret, J.-C. Bollinger, A. Hursthouse, *Acta Geochim.* **2021**, *40*, 466–471.

[94] J. Pilas, T. Selmer, M. Keusgen, M. J. Schöning, *Anal. Chem.* **2019**, *91*, 15293–15299.

[95] B. Attoye, C. Pou, E. Blair, C. Rinaldi, F. Thomson, M. J. Baker, D. K. Corrigan, *Biosensors* **2020**, *10*, 156.

[96] B. Attoye, M. J. Baker, F. Thomson, C. Pou, D. K. Corrigan, *Biosensors* **2021**, *11*, 42.

[97] P. Roberto de Oliveira, R. D. Crapnell, A. Garcia-Miranda Ferrari, P. Wuamprakhon, N. J. Hurst, N. C. Dempsey-Hibbert, M. Sawangphruk, B. C. Janegitz, C. E. Banks, *Biosens. Bioelectron.* **2023**, *228*, 115220.

[98] O. Ordeig, J. del Campo, F. X. Muñoz, C. E. Banks, R. G. Compton, *Electroanalysis* **2007**, *19*, 1973–1986.

[99] O. Ordeig, C. E. Banks, J. del Campo, F. X. Muñoz, R. G. Compton, *Electroanalysis* **2006**, *18*, 573–578.

[100] X.-J. Huang, A. M. O'Mahony, R. G. Compton, *Small* **2009**, *5*, 776–788.

[101] R. O. Kadara, N. Jenkinson, C. E. Banks, *Electrochem. Commun.* **2009**, *11*, 1377–1380.

[102] T. Kondo, I. Udagawa, T. Aikawa, T. Sakamoto, I. Shitanda, Y. Hoshi, M. Itagaki, M. Yuasa, *Anal. Chem.* **2016**, *88*, 1753–1759.

[103] S. R. Belding, J. G. Limon-Petersen, E. J. F. Dickinson, R. G. Compton, *Angew. Chem. Int. Ed.* **2010**, *49*, 9242–9245.

[104] R. G. Compton, C. E. Banks, *Understanding Voltammetry*, World Scientific **2018**.

[105] J. Wang, J. Lu, B. Tian, C. Yarnitzky, *J. Electroanal. Chem.* **1993**, *361*, 77–83.

[106] B. Seddon, Y. Shao, H. Girault, *Electrochim. Acta* **1994**, *39*, 2377–2386.

[107] S. Liébana, L. J. Jones, G. A. Drago, R. W. Pittson, D. Liu, W. Perrie, J. P. Hart, *Sens. Actuators B* **2016**, *231*, 384–392.

[108] C. Cugnet, O. Zaouak, A. René, C. Pécheyran, M. Potin-Gautier, L. Authier, *Sens. Actuators B* **2009**, *143*, 158–163.

[109] A. C. Barton, S. D. Collyer, F. Davis, D. D. Gornall, K. A. Law, E. C. D. Lawrence, D. W. Mills, S. Myler, J. A. Pritchard, M. Thompson, S. P. J. Higson, *Biosens. Bioelectron.* **2004**, *20*, 328–337.

[110] S. Myler, F. Davis, S. D. Collyer, S. P. Higson, *Biosens. Bioelectron.* **2004**, *20*, 408–412.

[111] F. Tan, J. P. Metters, C. E. Banks, *Sens. Actuators B* **2013**, *181*, 454–462.

[112] I. Streeter, N. Fietkau, J. del Campo, R. Mas, F. X. Muñoz, R. G. Compton, *J. Phys. Chem. C* **2007**, *111*, 12058–12066.

[113] K. C. Honeychurch, S. Al-Berezanchi, J. P. Hart, *Talanta* **2011**, *84*, 717–723.

[114] D. H. Craston, C. P. Jones, D. E. Williams, N. El Murr, *Talanta* **1991**, *38*, 17–26.

[115] F. J. Rawson, W. M. Purcell, J. Xu, D. C. Cowell, P. R. Fielden, N. Biddle, J. P. Hart, *Electrochim. Acta* **2007**, *52*, 7248–7253.

[116] J. P. Metters, R. O. Kadara, C. E. Banks, *Sens. Actuators B* **2012**, *169*, 136–143.

[117] J.-L. Chang, J.-M. Zen, *Electroanalysis* **2006**, *18*, 941–946.

[118] J.-L. Chang, J.-M. Zen, *Electrochem. Commun.* **2006**, *8*, 571–576.

[119] C. H. Chou, J. L. Chang, J. M. Zen, *Electroanal. Int. J. Devoted Fundam. Pract. Asp. Electroanal.* **2009**, *21*, 206–209.

[120] C.-H. Chou, J.-L. Chang, J.-M. Zen, *Sens. Actuators B* **2010**, *147*, 669–675.

[121] F. Rawson, W. Purcell, J. Xu, R. Pemberton, P. Fielden, N. Biddle, J. Hart, *Talanta* **2009**, *77*, 1149–1154.

[122] R. Pemberton, J. Xu, R. Pittson, N. Biddle, G. Drago, S. Jackson, J. Hart, *Anal. Biochem.* **2009**, *385*, 334–341.

[123] R. Pemberton, J. Xu, R. Pittson, G. Drago, J. Griffiths, S. Jackson, J. Hart, *Biosens. Bioelectron.* **2011**, *26*, 2448–2453.

[124] W.-C. Chen, P.-Y. Li, C.-H. Chou, J.-L. Chang, J.-M. Zen, *Electrochim. Acta* **2015**, *153*, 295–299.

[125] W.-C. Chen, Y.-L. Hsu, S. Venkatesan, J.-M. Zen, *Electroanalysis* **2014**, *26*, 565–572.

[126] J.-L. Chang, J.-M. Zen, *Electrochem. Commun.* **2007**, *9*, 2744–2750.

[127] O. Zaouak, L. Authier, C. Cugnet, A. Castetbon, M. Potin-Gautier, *Electroanalysis.* **2009**, *21*, 689–695.

[128] M. Y. Vagin, A. N. Sekretaryova, R. S. Reategui, I. Lundstrom, F. Winquist, M. Eriksson, *ChemElectroChem* **2014**, *1*, 755–762.

[129] L. Authier, C. Grossiord, P. Brossier, B. Limoges, *Anal. Chem.* **2001**, *73*, 4450–4456.

[130] A. Konash, A. R. Harris, J. Zhang, D. Elton, M. Hyland, G. Kennedy, A. M. Bond, *J. Solid State Electrochem.* **2009**, *13*, 551–563.

[131] R. Pemberton, R. Pittson, N. Biddle, J. Hart, *Biosens. Bioelectron.* **2009**, *24*, 1246–1252.

[132] A. N. Sekretaryova, A. V. Volkov, I. V. Zozoulenko, A. P. F. Turner, M. Y. Vagin, M. Eriksson, *Anal. Chim. Acta* **2016**, *907*, 45–53.

[133] J. P. Metters, E. P. Randviir, C. E. Banks, *Analyst* **2014**, *139*, 5339–5349.

[134] A. P. Ruas de Souza, C. W. Foster, A. V. Kolliopoulos, M. Bertotti, C. E. Banks, *Analyst* **2015**, *140*, 4130–4136.

[135] A. P. Ruas de Souza, M. Bertotti, C. W. Foster, C. E. Banks, *Electroanalysis* **2015**, *27*, 2295–2301.

[136] Y. Liu, J. Pan, Z. Hu, Y. Chu, M. S. Khan, K. Tang, L. Guo, C. Lau, *Microchim. Acta* **2020**, *187*, 664.

[137] A. Kaliyaraj Selva Kumar, Y. Zhang, D. Li, R. G. Compton, *Electrochem. Commun.* **2020**, *121*, 106867.

[138] Y. Zhang, A. K. Selva Kumar, D. Li, M. Yang, R. G. Compton, *ChemElectroChem* **2020**, *7*, 4614–4624.

[139] K. C. Honeychurch, L. Gilbert, J. P. Hart, *Anal. Bioanal. Chem.* **2010**, *396*, 3103–3111.

[140] J. P. Hart, I. C. Hartley, *Analyst* **1994**, *119*, 259–263.

[141] S. A. Wring, J. P. Hart, B. J. Birch, *Electroanalysis* **1992**, *4*, 299–309.

[142] T. Shimomura, T. Sumiya, M. Ono, T. Ito, T.-A. Hanaoka, *Anal. Chim. Acta* **2012**, *714*, 114–120.

[143] A. Smart, K. L. Westmacott, A. Crew, O. Doran, J. P. Hart, *Biosensors* **2019**, *9*, 98.

[144] A. Crew, D. Lonsdale, N. Byrd, R. Pittson, J. Hart, *Biosens. Bioelectron.* **2011**, *26*, 2847–2851.

[145] A. Smart, A. Crew, O. Doran, J. P. Hart, *J. Food Compos. Anal.* **2023**, *122*, 105488.

[146] A. Smart, A. Crew, O. Doran, J. P. Hart, *Appl. Sci.* **2020**, *10*, 7779.

[147] N. Hernández-Ibáñez, I. Sanjuán, M. Á. Montiel, C. W. Foster, C. E. Banks, J. Iniesta, *J. Electroanal. Chem.* **2016**, *780*, 303–310.

[148] R. O. Kadara, N. Jenkinson, C. E. Banks, *Electroanalysis* **2009**, *21*, 2410–2414.

[149] M. Khairy, R. O. Kadara, D. K. Kampouris, C. E. Banks, *Electroanalysis* **2010**, *22*, 1455–1459.

[150] R. O. Kadara, I. E. Tothill, *Anal. Chim. Acta* **2008**, *623*, 76–81.

[151] A. F. Khan, A. G.-M. Ferrari, J. P. Hughes, G. C. Smith, C. E. Banks, S. J. Rowley-Neale, *Sensors* **2022**, *22*, 3330.

[152] S. J. Rowley-Neale, G. C. Smith, C. E. Banks, *ACS Appl. Mater. Interfaces* **2017**, *9*, 22539–22548.

[153] S. J. Rowley-Neale, C. W. Foster, G. C. Smith, D. A. C. Brownson, C. E. Banks, *Sustain. Energy Fuels* **2017**, *1*, 74–83.

[154] J. P. Hughes, F. D. Blanco, C. E. Banks, S. J. Rowley-Neale, *RSC Adv.* **2019**, *9*, 25003–25011.

[155] J. P. Hughes, S. Rowley-Neale, C. Banks, *RSC Adv.* **2021**, *11*, 8073–8079.

[156] S. J. Rowley-Neale, D. A. C. Brownson, G. Smith, C. E. Banks, *Biosensors* **2020**, *10*, 27.

[157] S. A. Atty, A. H. Ibrahim, E. M. Hussien, *J. Electrochem. Soc.* **2019**, *166*, B1483.

[158] E. Turkusic, V. Milicevic, H. Tahmiscija, M. Vehabovic, S. Basic, V. Amidzic, *Fresenius J. Anal. Chem.* **2000**, *368*, 466–470.

[159] F. Ghamouss, S. Ledru, N. Ruillé, F. Lantier, M. Boujtita, *Anal. Chim. Acta* **2006**, *570*, 158–164.

[160] M. Caldara, J. W. Lowdon, G. van Wissen, A. G.-M. Ferrari, R. D. Crapnell, T. J. Cleij, H. Diliën, C. E. Banks, K. Eersels, B. van Grinsven, *Adv. Mater. Interfaces* **2023**, *10*, 2300182.

[161] P. Shivappa Adarakatti, C. W. Foster, C. E. Banks, A. K. N. S. P. Malingappa, *Sens. Actuators A* **2017**, *267*, 517–525.

[162] M. P. Down, S. J. Rowley-Neale, G. C. Smith, C. E. Banks, *ACS Appl. Energ. Mater.* **2018**, *1*, 707–714.

[163] B. Crane, J. P. Hughes, S. J. Rowley Neale, M. Rashid, P. E. Linton, C. E. Banks, K. J. Shaw, *Analyst* **2021**, *146*, 5574–5583.

[164] M. P. O'Halloran, M. Pravda, G. G. Guilbault, *Talanta* **2001**, *55*, 605–611.

[165] J. A. Bonacin, P. L. Dos Santos, V. Katic, C. W. Foster, C. E. Banks, *Electroanalysis* **2018**, *30*, 170–179.

ChemElectroChem

Review

doi.org/10.1002/celc.202400370

Chemistry Europe
European Chemical
Societies Publishing

[166] M. Singh, N. Jaiswal, I. Tiwari, C. W. Foster, C. E. Banks, *J. Electroanal. Chem.* **2018**, *829*, 230–240.

[167] M. Singh, I. Tiwari, C. W. Foster, C. E. Banks, *Mater. Res. Bull.* **2018**, *101*, 253–263.

[168] E. Turkusic, J. Kalcher, E. Kahrovic, N. W. Beyene, H. Moderegger, E. Sofic, S. Begic, K. Kalcher, *Talanta* **2005**, *65*, 559–564.

[169] I. Tiwari, M. Singh, M. Gupta, J. P. Metters, C. E. Banks, *Anal. Methods* **2015**, *7*, 2020–2027.

[170] M. Pravda, M. P. O'Halloran, M. P. Kreuzer, G. G. Guilbault, *Anal. Lett.* **2002**, *35*, 959–970.

[171] R. Pauliukaite, R. Metelka, I. Švancara, A. Królicka, A. Bobrowski, E. Norkus, K. Kalcher, K. Vytřas, *Sci. Pap. Univ. Pardubice Ser. A* **2004**, *10*, 47–58.

[172] R. Gusmão, V. López-Puente, I. Pastoriza-Santos, J. Pérez-Juste, M. F. Proença, F. Bento, D. Geraldo, M. C. Paiva, E. González-Romero, *RSC Adv.* **2015**, *5*, 5024–5031.

[173] Y. L. Su, C. Y. Tai, J. M. Zen, *Electroanalysis* **2013**, *25*, 2539–2546.

[174] S. Wang, K. Chang, C.-J. Yuan, *Electrochim. Acta* **2009**, *54*, 4937–4943.

[175] G. Cui, J. H. Yoo, J. S. Lee, J. Yoo, J. H. Uhm, G. S. Cha, H. Nam, *Analyst* **2001**, *126*, 1399–1403.

[176] J. Wang, M. Pedrero, H. Sakslund, O. Hammerich, J. Pingarron, *Analyst* **1996**, *121*, 345–350.

[177] H. Wei, J.-J. Sun, Y. Xie, C.-G. Lin, Y.-M. Wang, W.-H. Yin, G.-N. Chen, *Anal. Chim. Acta* **2007**, *588*, 297–303.

[178] D. Pan, S. Rong, G. Zhang, Y. Zhang, Q. Zhou, F. Liu, M. Li, D. Chang, H. Pan, *Electrochemistry* **2015**, *83*, 725–729.

[179] N. Raja, T. Kokulnathan, S.-M. Chen, W.-C. Liao, T. S. Priya, *Int. J. Electrochem. Sci.* **2017**, *12*, 4620–4629.

[180] M. I. González-Sánchez, B. Gómez-Monedero, J. Agrisuelas, J. Iniesta, E. Valero, *J. Electroanal. Chem.* **2019**, *839*, 75–82.

[181] Y.-J. Chen, T.-H. Yang, J.-L. Chang, W.-L. Cheng, A. S. Kumar, J.-M. Zen, *J. Electroanal. Chem.* **2019**, *839*, 59–66.

[182] L. R. Cumba, C. W. Foster, D. A. C. Brownson, J. P. Smith, J. Iniesta, B. Thakur, D. R. do Carmo, C. E. Banks, *Analyst* **2016**, *141*, 2791–2799.

[183] D. Stan, A.-C. Mirica, R. Iosub, D. Stan, N. B. Mincu, M. Gheorghe, M. Avram, B. Adiaconita, G. Craciun, A. L. Bocancia Mateescu, *Processes* **2022**, *10*, 723.

[184] S. A. Wring, J. P. Hart, L. Bracey, B. J. Birch, *Anal. Chim. Acta* **1990**, *231*, 203–212.

[185] R. D. Crapnell, A. Garcia-Miranda Ferrari, M. J. Whittingham, E. Sigley, N. J. Hurst, E. M. Keefe, C. E. Banks, *Sensors* **2022**, *22*, 9521.
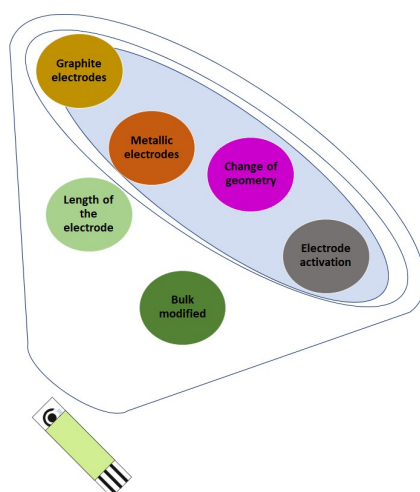
REVIEW

In our paper we overview the use of screen-printed electrode focusing on metallic and bulk modified varieties, geometric changes (micro, microband and associated arrays), electrode activation and finally the physical length of screen-printed electrodes, providing insights for future research.

*R. D. Crapnell, C. E. Banks**

1 – 23

Electroanalytical Overview: Screen-Printed Electrochemical Sensing Platforms